BBA - General Subjects 1862 (2018) 2714–2727

Contents lists available at ScienceDirect

BBA - General Subjects

journal homepage: www.elsevier.com/locate/bbagen

"Pinching" the ammonia tunnel of CTP synthase unveils coordinated catalytic and allosteric-dependent control of ammonia passage

Gregory D. McCluskey[a], Stephen L. Bearne[a,b,*]

[a] Department of Biochemistry and Molecular Biology, Dalhousie University, Halifax, NS B3H 4R2, Canada
[b] Department of Chemistry, Dalhousie University, Halifax, NS B3H 4R2, Canada

ARTICLE INFO

Keywords:
CTP synthase
Mutagenesis
Molecular gate
Ammonia tunnel
Kinetics, catalytic synchronization

ABSTRACT

Molecular gates within enzymes often play important roles in synchronizing catalytic events. We explored the role of a gate in cytidine-5′-triphosphate synthase (CTPS) from *Escherichia coli*. This glutamine amidotransferase catalyzes the biosynthesis of CTP from UTP using either L-glutamine or *exogenous* NH_3 as a substrate. Glutamine is hydrolyzed in the glutaminase domain, with GTP acting as a positive allosteric effector, and the *nascent* NH_3 passes through a gate located at the end of a ~25-Å tunnel before entering the synthase domain where CTP is generated. Substitution of the gate residue Val 60 by Ala, Cys, Asp, Trp, or Phe using site-directed mutagenesis and subsequent kinetic analyses revealed that V60-substitution impacts glutaminase activity, nucleotide binding, salt-dependent inhibition, and inter-domain NH_3 transport. Surprisingly, the increase in steric bulk present in V60F perturbed the local structure consistent with "pinching" the tunnel, thereby revealing processes that synchronize the transfer of NH_3 from the glutaminase domain to the synthase domain. V60F had a slightly reduced coupling efficiency at maximal glutaminase activity that was ameliorated by slowing down the glutamine hydrolysis reaction, consistent with a "bottleneck" effect. The inability of V60F to use exogenous NH_3 was overcome in the presence of GTP, and more so if CTPS was covalently modified by 6-diazo-5-oxo-L-norleucine. Use of NH_2OH by V60F as an alternative bulkier substrate occurred most efficiently when it was concomitant with the glutaminase reaction. Thus, the glutaminase activity and GTP-dependent activation act in concert to open the NH_3 gate of CTPS to mediate inter-domain NH_3 transport.

1. Introduction

Multi-domain enzymes often catalyze several different chemical reactions, and the chemistry at each site must be coordinated to limit the premature release of substrates and/or reaction intermediates. Indeed, many proteins contain tunnels and gates that are often highly dynamic structures that play an important role synchronizing catalytic events occurring at different locations during enzyme catalysis [1, 2]. Engineering of such protein gates and tunnels offers an attractive approach for rationally modifying the activity of enzymes, but requires a detailed understanding of how the opening and closing of such gates or tunnels are governed by ligand binding and/or catalytic events. The class I (or triad) subfamily of the glutamine-dependent amidotransferases, which catalyze the amination of ATP-activated substrates using the *nascent* NH_3 generated from the hydrolysis of L-glutamine (Gln), contain tunnels to facilitate efficient transfer of the NH_3 from its site of production to its site of utilization [3–8]. By and large, the glutaminase active sites are structurally similar among the subfamily members owing to the shared chemistry of the catalyzed step; however, the domains that catalyze the "downstream" amination (synthase) activity are unique to specific enzymes [9, 10]. As such, these enzymes furnish excellent models for understanding the evolution [11] and mechanism [12–17] of synchronization between multiple, and often distant, active sites.

Cytidine-5′-triphosphate (CTP) synthase (CTPS, EC 6.3.4.2) affords a particularly interesting example of a multi-domain, gated-amidotransferase, which must coordinate the hydrolysis of Gln in the C-terminal glutaminase (or GATase) domain [18] with the delivery of the resulting nascent NH_3 to the N-terminal synthase (or amidoligase) domain where it reacts with 4-phospho-UTP [19–21] to form CTP [22]

Abbreviations: CD, circular dichroism; CPS, carbamoyl phosphate synthase; CTPS, CTP synthase; Gln, L-glutamine; d_H, mean hydrodynamic diameter; DON, 6-diazo-5-oxo-L-norleucine; DLS, dynamic light scattering; *Ec*CTPS, CTPS from *Escherichia coli*; GlmS, glucosamine-6-phosphate synthase; MD, molecular dynamics; NadE, glutamine-dependent NAD^+ synthetase; NTP, nucleoside-5′-triphosphate; N^4-OH-CTP, N^4-hydroxy-CTP; SD, standard deviation

* Corresponding author at: Department of Biochemistry and Molecular Biology, Dalhousie University, Halifax, NS B3H 4R2, Canada.
E-mail address: sbearne@dal.ca (S.L. Bearne).

https://doi.org/10.1016/j.bbagen.2018.08.008
Received 11 June 2018; Received in revised form 20 July 2018; Accepted 6 August 2018
Available online 10 August 2018

(Fig. 1A). All these events must be properly synchronized to ensure that CTP is produced efficiently. As an added layer of complexity, CTPS is highly regulated by its nucleotide ligands. The substrates ATP and UTP promote oligomerization of the enzyme to active tetramers [22–24]. The product CTP can also effect this change in oligomerization state [25], as well as act as a feedback inhibitor [22, 26]. Because CTPS is the only known enzyme that catalyzes the de novo formation of CTP from UTP, and because CTP plays an important role in both membrane phospholipid [27–29] and nucleic acid biosynthesis [30], CTPS has been studied as a potential antiviral [31], antiprotozoal [32–38], antineoplastic, [30, 39] and immunosuppressive [40] drug target. Eukaryotic CTPS homologues have been shown to be regulated by phosphorylation [41–44] and, more recently, the enzyme has also been shown to form filaments both in vitro [45, 46] and in vivo [47], which may constitute an additional level of regulation [48–52]. Finally, guanosine-5′-triphosphate (GTP) is an allosteric activator of the glutaminase reaction [53] that induces a conformational change [54–57] stabilizing the tetrahedral intermediates formed during Gln hydrolysis [58] and may act as an activator in concert with the 4-phospho-UTP intermediate [21].

The X-ray crystal structures of CTPSs from *Escherichia coli* (*Ec*CTPS) [26, 59, 60] and *Mycobacterium tuberculosis* [61] revealed the presence of a 25-Å tunnel connecting the glutaminase and synthase domains that NH_3 must pass through during catalysis (Fig. 1). Although no structures of CTPS have been solved with bound GTP, or guanosine analogues, modeling studies suggest that GTP binds in the glutaminase domain at an opening leading to a solvent-filled "vestibule" that constitutes part of the NH_3 tunnel (Fig. 1C) [59]. CTPS can also utilize free (i.e., *exogenous*) NH_3 as a substrate, though the entry site for exogenous NH_3 has not been conclusively identified. That NH_3-dependent CTP generation is inhibited by GTP, however, suggests they may share a common binding site [62]. The NH_3 tunnel, starting in the glutaminase domain, is partially formed by the residues surrounding the catalytic triad (Glu 517–His 515–Cys 379) that catalyzes the hydrolysis reaction [58, 59, 63]. The tunnel continues to a constriction formed by 3 residues – Pro 54, His 57, and Val 60 – at the opening to the synthase domain that may comprise an NH_3 gate. These putative NH_3 gate residues are highly conserved among CTPSs (Fig. 2), and form the boundary between the glutaminase and synthase domains, suggesting that the gate plays a vital role in synchronizing the delivery of NH_3 to the preformed 4-phospho-UTP intermediate. His 57 is believed to function as a "door" that swings open or shut over the constriction, depending on whether or not UTP is bound [59]. According to high-resolution crystal structures of wild-type *Ec*CTPS and molecular models of the tunnel, the constriction is only ~2.4 Å in diameter [26, 59], despite the molecular diameter of NH_3 being closer to 4 Å [64]. Taking this into account, the tunnel captured in X-ray diffraction studies must undergo a conformational change to allow for the effective transfer of NH_3 to the synthase domain, or the constriction is an artefact of the crystallization conditions. The proximity of the gate to the putative GTP binding site suggests a possible role for GTP in regulating opening of the NH_3 gate, thus coupling spatially distant reactions by modulating the interdomain flow of NH_3.

Using site-directed mutagenesis, we replaced Val 60 of *Ec*CTPS by five amino acids (Ala, Cys, Asp, Trp, and Phe) at the most constricted part of the tunnel. We then employed a combination of kinetics and biophysical analyses to investigate the role of Val 60 in interdomain NH_3 transport. While the substitutions revealed the exquisite sensitivity of the enzyme to changes at the interface between its glutaminase and synthase domains, the Phe substitution unveiled the coordinated role of GTP binding *and* the glutaminase activity in facilitating passage of NH_3 through the tunnel gate, thereby suggesting an additional role for GTP as an allosteric effector.

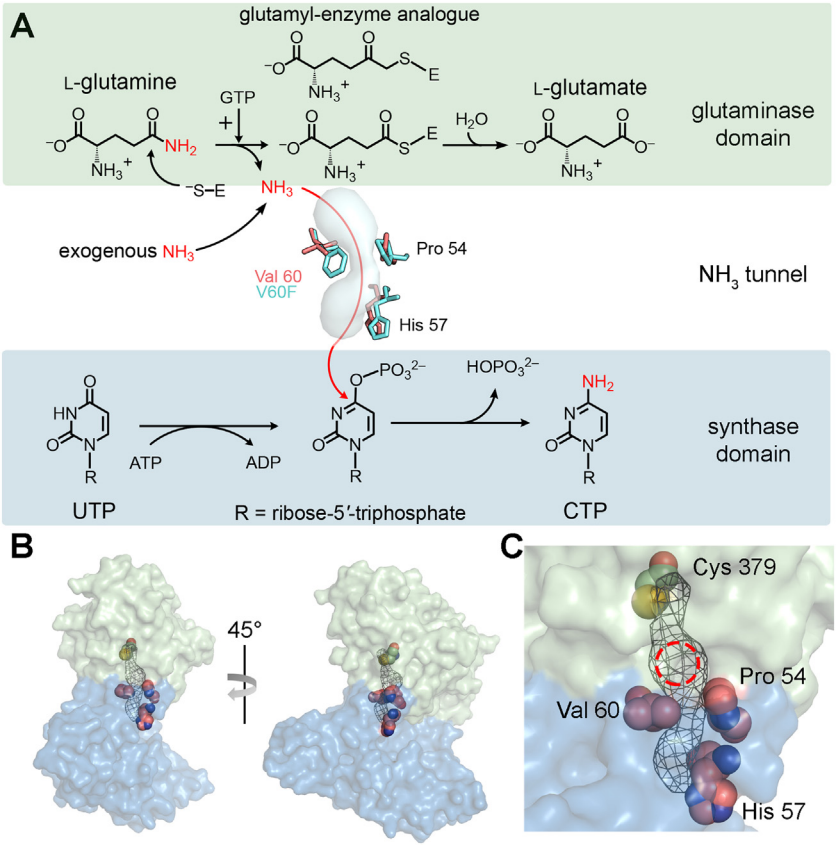

Fig. 1. Catalytic mechanism and mutation strategy for exploring inter-domain NH_3 transport in *Ec*CTPS. (A) The reaction catalyzed by CTPS involves the transfer of the nascent NH_3, generated through GTP-activated hydrolysis of L-glutamine (Gln) in the glutaminase domain, to the synthase domain where it reacts with UTP that has been activated through ATP-dependent phosphorylation at the 4-position to form CTP. The structural mimic of the glutamyl-enzyme intermediate formed following treatment of *Ec*CTPS with 6-diazo-5-oxo-L-norleucine (DON) is shown above the intermediate. Amino acid residues of the wild-type (red) and V60F (cyan) *Ec*CTPS variants comprising the putative NH_3 gate are shown as sticks alongside a tunnel model (surface) to illustrate the constriction. (B) The NH_3 tunnel (dark mesh) of an *Ec*CTPS monomer connects the glutaminase (green) and synthase (blue) domains. Amino acids making up the surface of *Ec*CTPS are depicted as surface representations with the tunnel modeled in mesh. The tunnel was modeled into the wild-type *Ec*CTPS structure (PDB 2AD5, [26]) using CAVER Analyst 1.0 [75] for PyMOL with a probe radius of 1.2 Å. (C) The NH_3 tunnel passes through a molecular gate comprised of Pro 54, His 57, and Val 60. The catalytic cysteine and amino acids making up the NH_3 gate (space-filling representations) are shown. The putative GTP-binding site is indicated by the dashed red circle and resides adjacent to the gate.

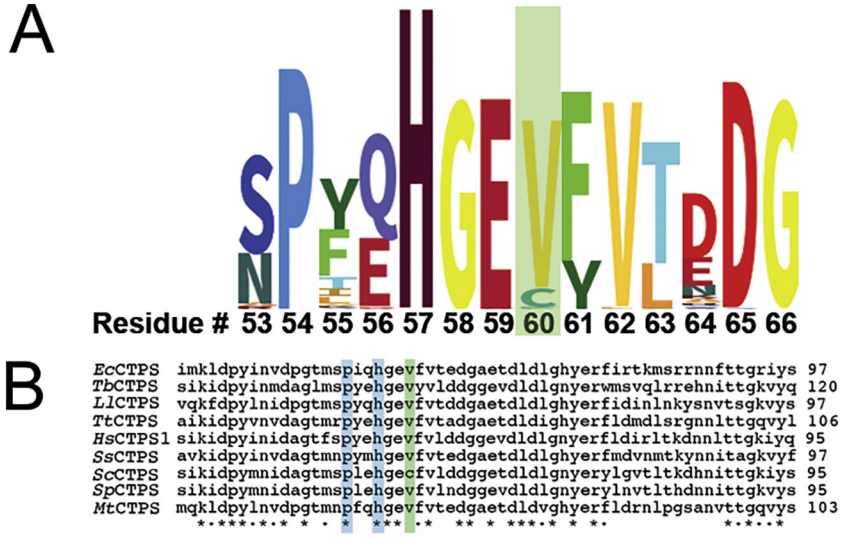

Fig. 2. Amino acid sequence neighboring the NH_3 gate residues. (A) Partial HMM logo for 5324 predicted CTP synthase protein sequences. Val 60 (*E. coli* numbering) is highlighted in green. Skylign [91] was employed to construct this hidden Markov model (HMM) logo from an alignment of 5324 predicted CTP synthase protein sequences obtained from the Pfam database [92]. The relative amino acid probabilities for positions 57 and 60 (*E. coli* numbering) are provided in Supplementary Tables S3 and S4, respectively. (B) Amino acid sequence alignment of a portion of 9 representative CTPSs containing a putative NH_3 tunnel. Invariant residues (*) and residues showing conservation between groups of strongly (:) or weakly (.) similar properties are indicated. Val 60 (green, *E. coli* numbering), Pro 54 (blue), and His 57 (blue) are highlighted. In descending order the proteins included in the alignment are as follows: *Escherichia coli* (taxid:562), *Trypanosoma brucei* (taxid:5691), *Lactococcus lactis* (taxid:1358), *Thermus thermophilus* (taxid:274), *Homo sapiens* (taxid:9606), *Sulfolobus solfataricus* (taxid:2287), *Saccharomyces cerevisiae* (taxid:4932), *Schizosaccharomyces pombe* (taxid:4896), and *Mycobacterium tuberculosis* (taxid:83332). Alignment rendering was conducted using Clustal Omega [93].

2. Materials and methods

2.1. General

All chemicals, unless stated otherwise, were purchased from Sigma-Aldrich Canada Ltd. (Oakville, ON, Canada). The pET-15b expression system (Novagen) and HisBind resin (Novagen) were purchased from EMD Millipore (Etobicoke, ON, Canada). Synthetic DNA oligonucleotides for site-directed mutagenesis were purchased from Integrated DNA Technologies (Coralville, IA). Plasmid preparations for site-directed mutagenesis and bacterial transformations were conducted using QIAprep Spin Mini-prep Kits (Qiagen, Toronto, ON, Canada). For HPLC experiments, a Waters 510 pump and 680 controller were used for solvent delivery, and injections were carried out with a Rheodyne 7725i sample injector fitted with a 20-μL injection loop. Analytes were detected with a Waters 474 scanning fluorescence detector or a Waters 486 absorbance detector, as indicated. Circular dichroism studies were carried out using a JASCO J-810 spectropolarimeter (Jasco Inc., Easton, MD).

2.2. Site-directed mutagenesis and enzyme purification

The pET-15b-CTPS1 plasmid [58], containing the CTPS open reading frame from *Escherichia coli*, was used as the template for site-directed mutagenesis. Site-directed mutagenesis was conducted using the QuickChange Site-Directed Mutagenesis Kit (Stratagene Inc., La Jolla, CA) with KAPA HiFi DNA polymerase (Kapa Biosystems, Wilmington, MA). The synthetic oligodeoxynucleotide primers are given in Supplementary Table S1. The entire plasmid open reading frame was commercially sequenced (Robarts Research, London, ON, Canada) to verify that no other mutations in the nucleotide sequence were introduced.

Wild-type and mutant forms of recombinant *Ec*CTPS were purified from *E. coli* BL21(DE3) cells transformed with either the pET-15b-CTPS1, pET-15b-CTPSH57A, pET-15b-CTPSV60A, pET-15b-CTPSV60C, pET-15b-CTPSV60D, pET-15b-CTPSV60W, or pET-15b-CTPSV60F plasmids as described previously [58]. Soluble *Ec*CTPS variants bearing an N-terminal His_6-tag were purified by metal ion affinity chromatography using established protocols [58] and dialyzed against Na^+-HEPES buffer (70 mM, pH 8.0) containing $MgCl_2$ (10 mM) and EGTA (0.5 mM) (i.e., assay buffer). Recombinant enzyme preparations were > 98% pure as determined by analysis using SDS-PAGE (8%) (see Supplementary Fig. S1). The His_6-tag was not removed from the recombinant enzymes since the tag does not affect the activity of the enzyme [58]. The concentration of each His_6-tagged *Ec*CTPS variant was determined from its absorbance at 280 nm using a molar extinction coefficient (ε) of 40,340 $M^{-1}\,cm^{-1}$ for all *Ec*CTPSs except for V60W *Ec*CTPS for which ε = 45,840 $M^{-1}\,cm^{-1}$. Molar extinction coefficients were calculated using the ProtParam tool available on the ExPASy server (http://web.expasy.org/protparam) [65].

2.3. Assay of CTP formation

The rate of *Ec*CTPS-catalyzed conversion of UTP to CTP was determined at 37 °C by following the change in absorbance at 291 nm (Δε = 1338 $M^{-1}\,cm^{-1}$) [22]. The reaction mixture contained *Ec*CTPS in assay buffer (70 mM Na^+-HEPES, pH 8.0, containing 10 mM $MgCl_2$ and 0.5 mM EGTA) and what was determined to be the saturating concentrations of ligands (Supplementary Table S2), unless stated otherwise. *Ec*CTPS (10–30 μg/mL for wild-type, V60A, V60C, V60D, V60W, and DON-V60F; 120–400 μg/mL for V60F) and nucleotides (Supplementary Table S2) were pre-incubated at 37 °C followed by the addition of the NH_3 source (NH_4Cl, NH_4OAc, or Gln) to initiate the reaction. For reactions using NH_4Cl or NH_4OAc (5.0–150 mM), KCl or NaOAc were used, respectively, to maintain the ionic strength at 0.15 M. The $[NH_3]$ present at pH 8.0 was calculated using a pK_a (NH_4^+) value of 9.24 (i.e., $[NH_3] = 0.0575 \cdot [NH_4Cl]_{total}$) [54]. For reactions using Gln (0.05–6.0 mM for wild-type, V60A, V60C, and V60D; 2–50 mM for V60F), GTP was present at saturating concentrations, unless stated otherwise (Supplementary Table S2). The concentrations of the *Ec*CTPS variants utilized in the assays were chosen so that reliable initial velocities could be measured. The values of K_m, k_{cat}, and k_{cat}/K_m were determined by fitting of Eq. (1) to the initial velocity data. The dependence of CTP formation on GTP (0–2.0 mM) was measured with either Gln (6.0 mM for wild-type, V60A, V60C, and V60D; 50.0 mM for V60F) or NH_4OAc (150 mM for DON-V60F). The values of k_{act}, K_A, and k_o were determined by fitting of Eq. (2) to the initial velocity data. The dependence of CTP formation on UTP (0–2.0 mM for wild-type; 0–4.0 mM for V60A, V60C, V60D, V60F, and DON-V60F; 0–5.0 mM for V60W) and ATP (0–4.0 mM) was examined with either Gln (6.0 mM for wild-type, V60A, V60C, and V60D; 50 mM for V60F) or NH_4OAc (150 mM for V60W and DON-V60F). All kinetic experiments with DON-V60F were conducted in the presence of a saturating concentration of GTP (1.0 mM), unless stated otherwise. Eq. (3) was fit to the initial velocity data using non-linear regression analysis to estimate the values of $V_{max}/[E]_T$, $[S]_{0.5}$, and n when ATP and UTP were examined as the variable substrates. Inhibition of Gln-dependent CTP formation by salts was determined by incubating the indicated *Ec*CTPS

variants with increasing concentrations of NaCl, KCl, or NaOAc (0–150 mM). Wild-type, V60A, V60C, V60D, and V60F *Ec*CTPSs were pre-incubated with saturating concentrations of GTP, ATP, and UTP (Supplementary Table S2) and the indicated concentration of salt. Reactions were initiated by addition of a saturating concentration of Gln (Supplementary Table S2) and Eq. (4) was fit to the relative velocity (v_i/v_o) data to estimate the IC_{50} and n values for the inhibition of the enzyme by salt.

$$v_i = \frac{k_{cat}[E]_T[S]}{K_m + [S]} \quad (1)$$

$$v_i = k_o + \frac{k_{act}[E]_T[GTP]}{K_A + [GTP]} \quad (2)$$

$$v_i = \frac{V_{max}[S]^n}{[S]^n_{0.5} + [S]^n} \quad (3)$$

$$\frac{v_i}{v_o} = \frac{IC_{50}^n}{IC_{50}^n + [I]^n} \quad (4)$$

2.4. Coupling ratio determinations

Glutaminase activities of the wild-type and Val 60 *Ec*CTPS variants were assayed by measuring the levels of Gln and glutamate derivatized by *o*-phthaldialdehyde in the presence of β-mercaptoethanol using RP-HPLC as described previously [57, 66]. Assays were conducted in assay buffer containing saturating concentrations of the appropriate ligands (Gln, GTP, ATP, and UTP) (Supplementary Table S2), and enzyme (3.0–5.0 μg/mL for wild-type, V60A, V60C, V60D, and V60W; 20–30 μg/mL for V60F) in a total volume of 1.0 mL. To investigate the integrity of the NH_3 tunnel, the coupling efficiency between the glutaminase and synthase active sites was calculated using Eq. (5) [57]. To investigate the "bottleneck" effect (vide infra) of V60F, Gln hydrolysis and CTP formation were determined using RP-HPLC and UV/vis spectroscopy, respectively, as described above except with saturating, near K_m, and sub-saturating concentrations of Gln. The coupling ratio was also determined at saturating concentrations of Gln, but with the concentration of GTP reduced to 0.006 mM for wild-type *Ec*CTPS and 0.08 mM for V60F (i.e., [GTP] ≈ K_A/5). For these glutaminase assays, the concentrations of wild-type *Ec*CTPS were 3.5 μg/mL (at saturating [Gln]), 6.9 μg/mL (at near K_m of Gln), 4.0 μg/mL (at sub-saturating [Gln]), and 3.9 μg/mL (at sub-saturating [GTP]); and the concentrations of V60F *Ec*CTPS were 10.0 μg/mL (at saturating [Gln]), 26.0 μg/mL (at near K_m of Gln), 23.7 μg/mL (at sub-saturating [Gln]), and 19.5 μg/mL (at sub-saturating [GTP]).

$$coupling\ ratio = \frac{(v_i/[E]_T)_{CTP\ formation}}{(v_i/[E]_T)_{Glu\ formation}} \quad (5)$$

2.5. Assay of N^4-OH-CTP formation

Competition between nascent and exogenous nitrogen sources was investigated using Gln as the source of nascent NH_3, and NH_2OH•HOAc as the exogenous nitrogen donor. NH_2OH•HCl was converted to the acetate salt [67] to avoid inhibition by chloride ions. Utilization of Gln or NH_2OH results in the conversion of UTP to either CTP or N^4-hydroxy-CTP (N^4-OH-CTP), which can be measured individually by monitoring the change in absorbance at 291 nm where, $\Delta\varepsilon_{291} = 1338\ M^{-1}\,cm^{-1}$ [22] or $\Delta\varepsilon_{291} = 4023\ M^{-1}\,cm^{-1}$ [68], respectively, or measured simultaneously by monitoring the change in absorbance at 291 nm and 300 nm where $\Delta\varepsilon_{300}$ for conversion of UTP to CTP is negligible and $\Delta\varepsilon_{300} = 3936\ M^{-1}\,cm^{-1}$ for the conversion of UTP to N^4-OH-CTP [68, 69]. Unlike ammonium salts, no calculation is needed to account for the total concentration of the nucleophilic form of NH_2OH because it has a pK_a value well below the assay pH of 8.0 (i.e., pK_a of $^+NH_3OH$ = 6.03 [70]). In the presence of both Gln and NH_2OH•HOAc, the initial rate of N^4-OH-CTP formation was calculated using $\Delta A_{300}/\Delta t$, while the initial rate of CTP formation was calculated using Eq. (6) [69], where l is the pathlength.

$$v_i = \frac{\Delta[CTP]}{\Delta t} = \frac{\Delta A_{291} - 1.73\Delta A_{300}}{\Delta t \Delta\varepsilon_{291} l} \quad (6)$$

To determine whether Gln and/or GTP could enhance utilization of exogenous NH_2OH, wild-type, V60F, and DON-V60F *Ec*CTPSs were assayed as described above with saturating concentrations of the indicated nucleotides (Supplementary Table S2). For wild-type *Ec*CTPS (40 μg/mL), the reaction was initiated by the addition of NH_2OH•HOAc (100 mM) alone, or simultaneously with Gln (6.0 mM). Similarly, reactions catalyzed by V60F and DON-V60F *Ec*CTPSs (110–125 μg/mL) were initiated by the addition of NH_2OH•HOAc (25 mM) alone, or simultaneously with Gln (50 mM). The ionic strength was maintained at 0.10 M using NaOAc for all variants. For wild-type *Ec*CTPS, Eqs. (7) and (8) were fit to the initial velocity data for CTP and N^4-OH-CTP formation, respectively, which were based on the kinetic mechanism shown in Supplementary Scheme S1. Due to substrate inhibition of V60F catalysis, Eq. (9) was fit to the initial velocity data for N^4-OH-CTP formation. Data are the average of three independent experiments ± SD.

$$\frac{d[CTP]/dt}{[E]_T} = \frac{(k_{cat}^{Gln} K_S^{NH2OH})}{K_S^{NH2OH} + [NH_2OH]} \quad (7)$$

$$\frac{d[N^4\text{-OH-CTP}]/dt}{[E]_T} = \frac{k_{cat}^{NH2OH}[NH_2OH]}{K_S^{NH2OH} + [NH_2OH]} \quad (8)$$

$$\frac{d[N^4\text{-OH-CTP}]/dt}{[E]_T} = \frac{k_{cat}^{NH2OH}[NH_2OH]}{K_S^{NH2OH} + [NH_2OH] + \frac{[NH_2OH]^2}{K_{NH2OH}}} \quad (9)$$

2.6. Derivatization of EcCTPS with 6-diazo-5-oxo-L-norleucine (DON)

To investigate whether acyl-enzyme formation could enhance the utilization of exogenous NH_3, the wild-type, V60A, and V60F *Ec*CTPSs (20 μM) were derivatized with DON (2.0 mM) in assay buffer containing ATP, UTP, and GTP (all NTPs at 1.0 mM) following the protocol of Koshland and co-workers [71, 72]. The reaction was incubated for 1 h at 37 °C prior to dialysis for 12 h against fresh assay buffer lacking NTPs. The resulting DON-modified variants were used immediately in kinetic assays. The effects of GTP on the utilization of exogenous NH_3 were investigated using unmodified wild-type *Ec*CTPS, DON-modified wild-type *Ec*CTPS (DON-*Ec*CTPS), DON-V60A, and DON-V60F (10–30 μg/mL) in assay buffer containing saturating concentrations of ligands (Supplementary Table S2) and NH_4OAc (150 mM) as the nitrogen donor. Eq. (4) was used to fit the initial velocity data for the inhibition of wild-type, DON-*Ec*CTPS, and DON-V60A *Ec*CTPSs. Activation of DON-V60F by GTP was analyzed using non-linear regression analysis by fitting of Eq. (2) to the initial velocity data.

2.7. Dynamic light scattering (DLS)

The oligomerization states of all the *Ec*CTPS variants were analyzed by DLS as previously described [52] using a BI-200SM goniometer and laser scattering system fitted with a Brookhaven Mini-L30 diode laser (637 nm, 30 mW; Brookhaven Instruments, Holtsville, NY). In brief, enzyme (30 μg/mL) was mixed with saturating concentrations of UTP and ATP (Supplementary Table S2) and filtered into a quartz cuvette. The filtered sample was equilibrated at 37 °C for 10 min prior to recording measurements at an angle of 60° for a total duration of 2 min at 37 °C. Intensity-weighted distributions of the hydrodynamic diameter (d_H) were acquired by fitting of a non-negative least squares (NNLS) algorithm to the autocorrelation functions using Brookhaven Instruments DLS software v. 5.89.

2.8. Tunnel modeling and molecular dynamics (MD) simulations

MD simulations were conducted on wild-type and V60F *Ec*CTPSs in order to gain structural insight into how the mutation might impact the overall protein structure, and how the tunnel might be constricted. Homology models for wild-type and V60F *Ec*CTPSs were built using SWISS-MODEL [73] to remove all ligands and restore missing residues that were not observed in the X-ray diffraction analysis of the original structure using a wild-type *Ec*CTPS structure as a template (PDB: 2AD5) [26]. The resulting 3D models were energy minimized prior to simulation using the method of steepest descent (50,000 steps, 100 ps) and a force constant of 1000 kJ mol^{-1} nm^{-2}. Each model was solvated using an explicit 3-point water model (SPC/E) in a cubic solute-box (143 × 143 × 143 Å). Simulations were conducted using GROMACS Version 5.0.4 with the GROMOS96 54a7 force field [74]. Temperature and pressure were maintained at 300 K and 1 atm, respectively. Bond lengths were constrained using the LINCS algorithm and all atoms of the system were subject to the dynamics simulation.

Initially, the V60F *Ec*CTPS model was simulated once for 10 ns with trajectory coordinates saved at 20-ps intervals. Wild-type and V60F *Ec*CTPS models were subsequently subjected to 100-ns simulations with no alterations to the other simulation parameters. Three-dimensional models of the NH_3 tunnel and statistical data were generated for the initial structures derived from the simulations, since the constriction present in V60F *Ec*CTPS became too great to model later in the simulation. CAVER Analyst 1.0 [75] was used to generate a 3D tunnel that passes through the NH_3 gate using the starting coordinates 107 × 95 × 52 Å, and the initial search area was set to 2 Å with a probe size of 0.6 Å. All other CAVER settings were kept as the defaults. For the wild-type *Ec*CTPS structure (PDB: 2AD5), the same coordinates were used, but with a probe size of 1.2 Å.

2.9. Circular dichroism (CD)

CD spectra for the *Ec*CTPS variants (0.2 mg/mL) in Tris-SO_4 buffer (2 mM, pH 8.0) containing $MgSO_4$ (10 mM) were obtained in triplicate over a wavelength range of 190–260 nm using a 0.1-cm light path at 37 °C. For each *Ec*CTPS variant, the average ellipticity of a buffer blank was subtracted from the observed average of ellipticity values obtained for the proteins.

2.10. Mass spectrometry (MS)

Both the V60F and DON-V60F *Ec*CTPS variants were analyzed using mass spectrometry. Gel bands from SDS-PAGE containing each variant were excised, processed, and analyzed using LC-ESI-MS/MS as described previously [76].

3. Results

To explore the role of the putative NH_3 gate in coordinating the reactions required for CTPS catalysis, we conducted site-directed mutagenesis to alter His 57 and Val 60. Substitution of the conserved His 57 "door" residue with alanine (H57A) yielded an *Ec*CTPS variant that retained the ability to hydrolyze Gln only 3-fold slower than wild-type *Ec*CTPS, but was unable to catalyze CTP formation (Supplementary Fig. S2). The fact that His is fully conserved at this position in CTPS homologues (Supplementary Table S3) suggests that this residue plays a critical role in catalysis. Because substitution of His 57 by Ala had such a detrimental effect on *Ec*CTPS-catalyzed CTP formation, we focused our attention on the gate residue Val 60, located at the most constricted part of the NH_3 tunnel. Examination of the sequence logo (Fig. 2) revealed that residues bearing short alkyl (Pro, Ile, and Ala) or neutral polar (Thr and Cys) side chains constitute the majority of (predicted) natural variants at position 60 (*E. coli* numbering), while larger, aromatic, and acidic or basic substitutions are not as abundant in the alignment (Supplementary Table S4). Consequently, we substituted Val 60 with a Phe residue with the anticipation that the increased steric bulk would block or impede the passage of NH_3 (Fig. 1A). Additionally, we substituted Val 60 with Ala, Cys, Asp, and Trp to examine the effects of some other side chains on catalysis. Though more "natural" substitutions (V60A and V60C) were well-tolerated, the V60D, V60W, and V60F substitutions were more disruptive to catalysis. With the exception of V60D, the Val 60-substituted *Ec*CTPS variants shared similar secondary structures as determined by circular dichroism spectroscopy (Supplementary Fig. S3).

3.1. NH_3-dependent CTP formation

Current high-resolution *Ec*CTPS structures reveal that the NH_3 tunnel contains a ~2.4-Å constriction that is primarily formed by the Pro-His-Val gate [26, 59]. These structures, therefore, do not depict active forms of the enzyme and conformational changes are required to open the NH_3 tunnel to permit passage of NH_3 (diameter ≈ 4 Å) [64]. To determine whether the ability of the *Ec*CTPS variants to utilize exogenous NH_3 as a substrate was affected by the amino acid substitutions, the kinetic parameters for NH_3-dependent CTP formation were determined (Table 1, Supplementary Figs. S4-S10). Conservative mutations (V60A and V60C) had minimal effect on the utilization of NH_3 derived from either NH_4Cl or NH_4OAc. The efficiency (k_{cat}/K_m) of

Table 1
Kinetic parameters for exogenous and nascent NH_3-dependent catalysis of wild-type and Val 60-substituted CTPS variants[a,b].

Nitrogen source	Kinetic parameter[c]	CTPS variant						
		Wild-type	V60A	V60C	V60D	V60W	V60F	DON-V60F
NH_4Cl-dependent CTP formation	K_m (mM)	2.15 ± 0.14[d]	0.7 ± 0.1	3.3 ± 0.7	3.6 ± 0.4	4.1 ± 2.2	–[e]	1.6 ± 0.3[f]
	k_{cat} (s^{-1})	9.50 ± 0.53[d]	3.3 ± 0.2	5.7 ± 0.8	0.99 ± 0.07	0.95 ± 0.31	–[e]	1.2 ± 0.1[f]
	k_{cat}/K_m (mM^{-1} s^{-1})	4.43 ± 0.12[d]	5.1 ± 1.2	1.8 ± 0.1	0.27 ± 0.01	0.25 ± 0.05	–[e]	0.73 ± 0.08[f]
NH_4OAc-dependent CTP formation	K_m (mM)	1.4 ± 0.1	0.61 ± 0.04	4.2 ± 0.2	1.6 ± 0.5	1.5 ± 0.1	0.94 ± 0.08[f]	3.1 ± 0.1[f]
	k_{cat} (s^{-1})	7.7 ± 0.5	3.12 ± 0.08	7.5 ± 0.2	1.1 ± 0.1	1.6 ± 0.1	0.16 ± 0.01[f]	2.2 ± 0.2[f]
	k_{cat}/K_m (mM^{-1} s^{-1})	5.3 ± 0.1	5.1 ± 0.2	1.8 ± 0.1	0.7 ± 0.2	1.1 ± 0.1	0.17 ± 0.01[f]	0.72 ± 0.05[f]
Gln-dependent CTP formation	K_m (mM)	0.24 ± 0.02[d]	0.37 ± 0.01	0.24 ± 0.04	0.5 ± 0.1	–[e]	5.9 ± 0.2	–[e]
	k_{cat} (s^{-1})	6.0 ± 0.4[d]	5.2 ± 0.2	5.14 ± 0.03	1.6 ± 0.2	–[e]	0.82 ± 0.06	–[e]
	k_{cat}/K_m (mM^{-1} s^{-1})	24.7 ± 0.7[d]	14.2 ± 0.9	21.6 ± 4.1	2.9 ± 0.5	–[e]	0.14 ± 0.01	–[e]

[a] See Supplementary Figs. S4–S10 for corresponding initial rate plots.
[b] See Supplementary Table S2 for the saturating concentrations of unvaried ligands.
[c] Values are the averages of three independent experiments ± SD.
[d] Data from reference [90].
[e] Activity too low to be determined reliably.
[f] Contained 1.0 mM GTP.

Table 2
Kinetic parameters for NTP-dependent catalysis of wild-type and Val 60-substituted *Ec*CTPS variants[a,b].

Activator/substrate	Kinetic parameter[c]	*Ec*CTPS variant						
		Wild-type	V60A	V60C	V60D	V60W[g]	V60F	DON-V60F[g]
GTP	K_A (mM)	0.03 ± 0.01[d]	0.15 ± 0.03	0.13 ± 0.01	0.78 ± 0.09	–[f]	0.42 ± 0.04	0.31 ± 0.02
	k_{act} (s^{-1})	7.1 ± 0.3[d]	5.9 ± 0.2	4.9 ± 0.2	1.31 ± 0.07	–[f]	1.0 ± 0.1	1.76 ± 0.03
	k_o (s^{-1})	0.5 ± 0.1	0.17 ± 0.03	0.3 ± 0.09	0.15 ± 0.02	–[f]	–[f]	0.25 ± 0.05
UTP	$[S]_{0.5}$	0.11 ± 0.01[d]	0.25 ± 0.02	0.15 ± 0.01	0.32 ± 0.05	1.2 ± 0.1	0.74 ± 0.08	1.00 ± 0.06
	$V_{max}/[E]_T$	4.2 ± 0.2[d]	5.69 ± 0.11	5.10 ± 0.03	1.7 ± 0.2	1.4 ± 0.1	1.05 ± 0.12	1.86 ± 0.09
	n	1.8 ± 0.1[d]	1.37 ± 0.08	1.4 ± 0.1	1.42 ± 0.06	2.16 ± 0.15	1.65 ± 0.08	1.75 ± 0.06
ATP	$[S]_{0.5}$	0.18 ± 0.04[e]	0.22 ± 0.01	0.19 ± 0.03	0.29 ± 0.02	0.96 ± 0.12	0.31 ± 0.06	0.47 ± 0.01
	$V_{max}/[E]_T$	5.6 ± 0.2 [e]	5.6 ± 0.3	5.1 ± 0.1	1.5 ± 0.1	1.46 ± 0.07	0.99 ± 0.06	1.68 ± 0.06
	n	1.5 ± 0.2[e]	1.29 ± 0.11	1.3 ± 0.1	1.54 ± 0.20	2.27 ± 0.08	2.0 ± 0.2	2.28 ± 0.14

[a] See Supplementary Figs. S4–S10 for corresponding initial rate plots.
[b] See Supplementary Table S2 for the saturating concentrations of unvaried ligands.
[c] Values are the averages of three independent experiments ± SD.
[d] Data from reference [90].
[e] Data from reference [52].
[f] Activity too low to be determined reliably.
[g] NTP-dependent kinetics for V60W and DON-V60F were measured with 150 mM NH_4OAc, while Gln was used as the NH_3 source for wild-type and all other *Ec*CTPS variants.

V60A (k_{cat}/K_m = 5.1 $mM^{-1}\,s^{-1}$) was slightly greater than that of wild-type *Ec*CTPS (k_{cat}/K_m = 4.43 $mM^{-1}\,s^{-1}$), owing to a higher affinity (decreased K_m) for exogenous NH_3, while V60C was slightly less efficient (k_{cat}/K_m = 1.8 $mM^{-1}\,s^{-1}$) due to a lower turnover number (k_{cat} = 5.7 s^{-1}). These observations suggest that small hydrophobic residues are required for optimal tunnel and/or gate function. Consistent with this hypothesis, V60D exhibited a much lower catalytic efficiency with exogenous NH_3 (k_{cat}/K_m = 0.27 $mM^{-1}\,s^{-1}$ (NH_4Cl) and 0.7 $mM^{-1}\,s^{-1}$ (NH_4OAc)) than wild-type *Ec*CTPS and the *Ec*CTPS variants bearing the conservative substitutions, though the K_m for NH_4Cl-derived NH_3 (3.6 mM) was 2-fold higher than that for NH_4OAc-derived NH_3 (1.6 mM), suggesting that the presence of Cl^- impaired NH_3 binding. Indeed, NaCl and KCl were more potent inhibitors of the Val 60-substituted *Ec*CTPSs, but acetate had much less impact than the chloride salts (Supplemental Fig. S11). V60W *Ec*CTPS had a K_m value with NH_4OAc-derived NH_3 (1.5 mM) similar to that of wild-type *Ec*CTPS, but the turnover number was approximately 5-fold lower (k_{cat} = 1.6 s^{-1}) (Table 1). Most interestingly, we found that V60F *Ec*CTPS was unable to use exogenous NH_3 as a substrate from either NH_4Cl or NH_4OAc. Only if GTP, which is normally an inhibitor of NH_3-dependent CTP formation [62], was added to the reaction mixture could CTP formation be detected. Even in the presence of GTP, the activity of V60F was only detectable with NH_4OAc due to the lack of concomitant inhibition by Cl^-, and the turnover (k_{cat}) and catalytic efficiency were about 50- and 30-fold lower (k_{cat} = 0.16 s^{-1}; k_{cat}/K_m = 0.17 $mM^{-1}\,s^{-1}$), respectively, than the values obtained for wild-type *Ec*CTPS (k_{cat} = 7.7 s^{-1}; k_{cat}/K_m = 5.3 $mM^{-1}\,s^{-1}$) (Table 1).

3.2. Gln-dependent CTP formation

As was observed for the effect of the substitutions on the kinetic parameters for NH_3-dependent CTP formation, the conservative substitutions (V60A and V60C) had little effect on catalysis when Gln was the substrate, unlike V60D, V60W, and V60F. The V60A and V60C variants had k_{cat}/K_m values of 14.2 and 21.6 $mM^{-1}\,s^{-1}$, respectively, similar to the wild-type efficiency of 24.7 $mM^{-1}\,s^{-1}$ (Table 1, Supplementary Figs. S4-S10). Neither the affinity of V60A and V60C *Ec*CTPSs for glutamine (K_m = 0.37 mM and 0.24 mM, respectively) nor their turnover values (k_{cat} = 5.2 s^{-1} and 5.14 s^{-1}, respectively) differed significantly from those of wild-type *Ec*CTPS (K_m = 0.24 mM; k_{cat} = 6.0 s^{-1}). On the other hand, V60D *Ec*CTPS exhibited an 8-fold decrease in catalytic efficiency (k_{cat}/K_m = 2.9 $mM^{-1}\,s^{-1}$), and the rates of Gln-dependent CTP formation catalyzed by V60W *Ec*CTPS were too low to be measured reliably (Table 1). Despite its inability to utilize exogenous NH_3 effectively as a substrate, V60F *Ec*CTPS could utilize Gln as a substrate, albeit its efficiency was reduced ~176-fold (k_{cat}/K_m = 0.14 $mM^{-1}\,s^{-1}$) relative to wild-type *Ec*CTPS. This marked reduction in catalytic efficiency arose from a 7-fold decrease in the turnover number (k_{cat} = 0.82 s^{-1}) and a 25-fold increase in K_m (5.9 mM), relative to wild-type *Ec*CTPS (Table 1).

Because Gln-dependent CTP formation requires the presence of the allosteric effector GTP for full activity, the GTP-dependent activation parameters were measured for each *Ec*CTPS variant (Table 2). Every substitution for Val 60 caused a reduction in the GTP-binding affinity ($1/K_A$). V60A (K_A = 0.15 mM) and V60C (K_A = 0.13 mM) *Ec*CTPSs had 5- and 4-fold reduced affinities for GTP, respectively, relative to wild-type *Ec*CTPS (K_A = 0.03 mM), though the activation rate constant (k_{act}) was similar to that of wild-type *Ec*CTPS for both variants (Table 2). Notably, the GTP-binding affinity for V60D (K_A = 0.78 mM) and V60F (K_A = 0.42 mM) *Ec*CTPSs were 24- and 13-fold weaker, respectively, than the GTP-binding affinity of wild-type *Ec*CTPS. Moreover, the activation rate constants were reduced 5- and 7-fold for V60D and V60F, respectively, relative to wild-type *Ec*CTPS, indicating that the acidic and bulky aromatic substitutions were detrimental to GTP-dependent activation of Gln-dependent CTP formation. The GTP-dependent kinetics could not be measured reliably for V60W *Ec*CTPS because of the inability of this variant to utilize Gln as a substrate. Clearly, amino acid substitutions at position 60 all cause local structural perturbations that have a detrimental effect on the ability of GTP to bind and activate the enzyme. This effect is in accord with notion that the putative GTP binding site is located near Val 60 [54, 57, 59, 77].

3.3. UTP- and ATP-dependent kinetics

UTP and ATP are not only required as substrates, but also promote oligomerization of the enzyme to form the active tetramers [24]. Val 60 is located near the dimer-dimer interface, and may also be close-enough to the synthase domain such that the Val 60-substituted variants might have impaired affinity for these NTP substrates. The UTP- and ATP-dependent kinetics were measured using Gln as the NH_3 source to explore this possibility, except for V60W *Ec*CTPS where its inability to utilize Gln as a substrate necessitated the use of NH_4OAc instead. All variants had very similar $[S]_{0.5}$ values for ATP binding ($[S]_{0.5} \approx$ 0.2–0.3 mM), with the exception of V60W *Ec*CTPS, which had a 5-fold lower affinity relative to wild-type *Ec*CTPS (Table 2, Supplementary Figs. S4-S10). On the other hand, the UTP-binding site

Table 3
Coupling efficiencies for wild-type and Val 60-substituted *Ec*CTPSs at saturating ligand concentrations[a,b].

	*Ec*CTPS variant					
	Wild-type	V60A	V60C	V60D	V60W	V60F
CTP formation ($v_i/[E]_T$, s^{-1})[c]	6.0 ± 0.4	4.74 ± 0.24	5.14 ± 0.03	1.39 ± 0.16	–[e]	0.85 ± 0.12
Gln hydrolysis ($v_i/[E]_T$, s^{-1})[c]	5.99 ± 0.23	3.8 ± 0.3	5.2 ± 0.7	1.27 ± 0.14	0.08 ± 0.02	1.14 ± 0.09
coupling efficiency[d]	1.00 ± 0.08	1.15 ± 0.17	0.99 ± 0.13	1.09 ± 0.15	N/A	0.75 ± 0.12

[a] See Supplementary Table S2 for saturating ligand concentrations.
[b] See Supplementary Fig. S12 for representative kinetic plots.
[c] Values are the averages of three independent experiments ± SD.
[d] Coupling efficiencies were calculated using Eq. (5).
[e] Activity too low to be detected.

appeared to be more sensitive to changes at residue position 60. Although the variants with the conservative substitutions (V60A and V60C) exhibited similar UTP-dependent turnover numbers compared to wild-type *Ec*CTPS ($V_{max}/[E]_T \approx 5–6\ s^{-1}$), substitution of Val 60 with a an acidic residue (V60D) or a large aromatic residue (V60W and V60F) caused an approximately 4-fold reduction in the turnover numbers (Table 2). Interestingly, only the substitutions with amino acids with bulky side chains cause a marked reduction in the UTP-binding affinity of 11- and 7-fold for V60W ($[S]_{0.5} = 1.2$ mM) and V60F ($[S]_{0.5} = 0.74$ mM) *Ec*CTPSs, respectively, relative to wild-type *Ec*CTPS ($[S]_{0.5} = 0.11$ mM). Overall, these data indicated that the less conservative substitutions for Val 60 had a greater impact on the synthase active site(s) than the more "natural" V60A and V60C mutations.

3.4. Glutaminase activity and coupling efficiencies

While the passage of *exogenous* NH_3 appeared to be blocked within the V60F *Ec*CTPS variant, *nascent* NH_3 was able to traverse the NH_3 tunnel to yield CTP, albeit at a much lower rate than wild-type *Ec*CTPS. The low rate of Gln-dependent CTP formation could have arisen from the added steric bulk of the Phe residue at position 60 of V60F causing a deformation in the tunnel leading to loss of nascent NH_3 directly from the tunnel (i.e., a leaky tunnel), or a more extensive effect on the glutaminase and/or synthase machinery. We determined the efficiency of NH_3 transport from the glutaminase domain to the synthase domain for the wild-type and Val 60-substituted *Ec*CTPSs by measuring the number of CTP molecules formed per molecule of NH_3 arising from Gln (i.e., coupling ratio, Eq. (5)). Like wild-type *Ec*CTPS, the V60A, V60C, and V60D variants all exhibited ~100% coupling efficiency (Table 3, Supplementary Fig. S12), indicating that the NH_3 tunnel was intact. However, V60D *Ec*CTPS exhibited reduced overall glutaminase activity relative to wild-type *Ec*CTPS, which accounted for its lower rate of CTP formation when using Gln as a substrate (Tables 1 and 3). Similarly, though we were unable to determine a coupling efficiency for V60W *Ec*CTPS since the Gln-dependent CTP formation was not measurable, the glutaminase activity for the V60W variant was very low ($k_{cat} \approx v_i/[E]_T = 0.08\ s^{-1}$, Table 3). The relatively high rate of activity with exogenous NH_3, but poor catalysis of Gln hydrolysis, suggested that the glutaminase reaction was somehow compromised by the substitution by Trp.

V60F *Ec*CTPS was the only Val 60 variant that exhibited a defect in NH_3 transport. At saturating concentrations of Gln, V60F *Ec*CTPS produced nascent NH_3 at a rate 1.3-fold faster than the rate at which CTP was formed, resulting in a coupling efficiency of 75% (Table 3). This reduced coupling efficiency could arise from either NH_3 leaking away from the tunnel or a "bottleneck" effect in which a rapid build-up of NH_3 occurs within the tunnel because of congestion at the now-constricted gate. We slowed the glutaminase reaction down by reducing the concentrations of either Gln or GTP to explore this possibility (Table 4, Supplementary Fig. S12). At concentrations of Gln near its K_m value, wild-type and V60F *Ec*CTPSs had coupling efficiencies of 98% and 105%, respectively, indicating that the overall rate of CTP generation was not substantially different from the rate of NH_3 formation in the glutaminase domain. At sub-saturating concentrations of Gln, the V60F substitution failed to block inter-domain coupling as well, since 100% of the nascent NH_3 was converted into CTP (Table 4). These data suggested that the V60F substitution did not introduce a leak, nor did it hinder the passage of nascent NH_3, except slightly when the rate of NH_3 formation was high. Moreover, this "bottleneck" effect was also relieved by slowing the rate of formation of the nascent NH_3 by reduction of the concentration of GTP at saturating concentrations of Gln. These observations indicate that the inability of the enzyme to efficiently transfer the NH_3, produced at high rates of Gln hydrolysis, from the glutaminase domain to the synthase domain was indeed the cause of the reduced NH_3 transfer in the V60F variant (Table 4). Still, the rate of Gln hydrolysis catalyzed by V60F *Ec*CTPS at saturating concentrations of Gln ($v_i/[E]_T = 1.14\ s^{-1}$) was lower than that of wild-type *Ec*CTPS ($v_i/[E]_T = 5.99\ s^{-1}$) by ~5-fold, indicating that the glutaminase reaction was also impaired by the V60F substitution (Table 3). The possibility that the V60F mutation introduces a pronounced alteration in the

Table 4
Coupling efficiencies for wild-type and V60F *Ec*CTPS at non-saturating concentrations of Gln or GTP[a,b].

*Ec*CTPS variant	[Gln] ≈ K_m[c]		Sub-saturating [Gln][c]		Sub-saturating [GTP][d]	
	Wild-type	V60F	Wild-type	V60F	Wild-type	V60F
CTP formation ($v_i/[E]_T$, s^{-1})[e]	3.32 ± 0.05	0.44 ± 0.03	0.33 ± 0.01	0.24 ± 0.01	1.44 ± 0.11	0.25 ± 0.02
Gln hydrolysis ($v_i/[E]_T$, s^{-1})[e]	3.38 ± 0.2	0.42 ± 0.09	0.31 ± 0.01	0.24 ± 0.02	1.42 ± 0.02	0.27 ± 0.02
coupling efficiency[f]	0.98 ± 0.06	1.05 ± 0.23	1.06 ± 0.05	1.00 ± 0.09	1.01 ± 0.08	0.93 ± 0.08
[Gln] (mM)	0.3	8.0	0.03	1.2	6.0	50.0

[a] Cf. the saturating concentrations of Gln were 6.0 mM and 50.0 mM for wild-type and V60F, respectively (Supplementary Table S2).
[b] See Supplementary Fig. S12 for representative kinetic plots.
[c] [GTP] = 1.0 mM
[d] [GTP] = 0.006 mM and 0.080 mM (i.e., [GTP] ≈ K_A/5) for wild-type and V60F *Ec*CTPSs, respectively.
[e] Values are the averages of three independent experiments ± SD.
[f] Coupling efficiencies were calculated using Eq. (5).

structure of the glutaminase domain could not be ruled out; though, circular dichroism spectroscopy of V60F *Ec*CTPS showed no appreciable difference in its secondary structure relative to wild-type *Ec*CTPS (Supplementary Fig. S3).

3.5. Utilization of exogenous NH_2OH

Evidently, *exogenous* NH_3 failed to be utilized as a substrate by V60F *Ec*CTPS in the absence of GTP, but *nascent* NH_3 was, somehow, able to overcome the effect of the V60F substitution. Because the passage of nascent NH_3 through the tunnel occurs in the presence of bound GTP and Gln hydrolysis within the glutaminase domain, we assessed whether Gln and/or GTP could enhance exogenous NH_3-dependent catalysis using an approach similar to that described by Willemöes for studies on the activation of CTPS from *Lactococcus lactis* [69]. In brief, NH_2OH may be used as an exogenous nitrogen source resulting in the formation of N^4-OH-CTP, which absorbs light at a higher wavelength than CTP allowing for the simultaneous determination of CTP or N^4-OH-CTP produced from nascent or exogenous nitrogen sources, respectively. However, we first had to establish that nascent (NH_3) and exogenous (NH_2OH) amines follow the same route in the *E. coli* homologue in order to draw a comparison between how the two sources are affected by Gln. For wild-type *Ec*CTPS, the rate of CTP formation arising from nascent NH_3 declined with a corresponding rise in N^4-OH-CTP as the concentration of NH_2OH was increased (Fig. 3A), suggesting that the two nucleophilic amines (NH_3 and NH_2OH) compete for reaction with the 4-phospho-UTP intermediate. When the same experiment was conducted using V60F *Ec*CTPS, N^4-OH-CTP formation was much slower, as might be expected due to the increased bulk of NH_2OH and the presumably obstructed tunnel; however, CTP formation from nascent NH_3 was strongly inhibited by increasing concentrations of NH_2OH, like wild-type *Ec*CTPS (Fig. 3B).

Having concluded that both nascent and exogenous amines likely take the same route to the synthase domain, we incubated V60F *Ec*CTPS with NH_2OH in the presence and absence of GTP and/or Gln to determine whether GTP binding and/or the glutaminase activity enhances the passage of exogenous NH_2OH to the synthase domain. In the presence of a saturating concentration of Gln, the rate of N^4-OH-CTP formation was enhanced ~3-fold more than with NH_2OH alone (Fig. 3C). However, unlike when NH_4OAc was the exogenous amine (Table 1), GTP alone was not able to enhance the utilization of the bulkier NH_2OH. Wild-type *Ec*CTPS did not exhibit any Gln- or GTP-dependent increase in NH_2OH utilization (Fig. 3C), consistent with the observation that the enzyme can efficiently utilize either exogenous NH_3 or NH_2OH as substrates and their passage to the synthase site is, therefore, normally unimpeded [57].

3.6. Effects of acyl-enzyme formation

Although the utilization of exogenous NH_2OH by V60F *Ec*CTPS increased upon addition of Gln, whether the enhanced rate of N^4-OH-CTP formation arose because of concomitant Gln binding or hydrolysis was ambiguous. *Ec*CTPS catalyzes the hydrolysis of Gln at a basal rate in the absence of GTP, thus either binding or hydrolysis of Gln may have enhanced NH_2OH utilization. During Gln hydrolysis, the side chain thiolate of Cys 379 acts as the nucleophile forming a glutamyl-enzyme intermediate and releasing NH_3. The thioester intermediate is subsequently hydrolyzed yielding Glu [58, 63]. To ascertain whether formation of the glutamyl-enzyme intermediate (Fig. 1A) formed during the hydrolysis of Gln enhanced the utilization of an exogenous nitrogen

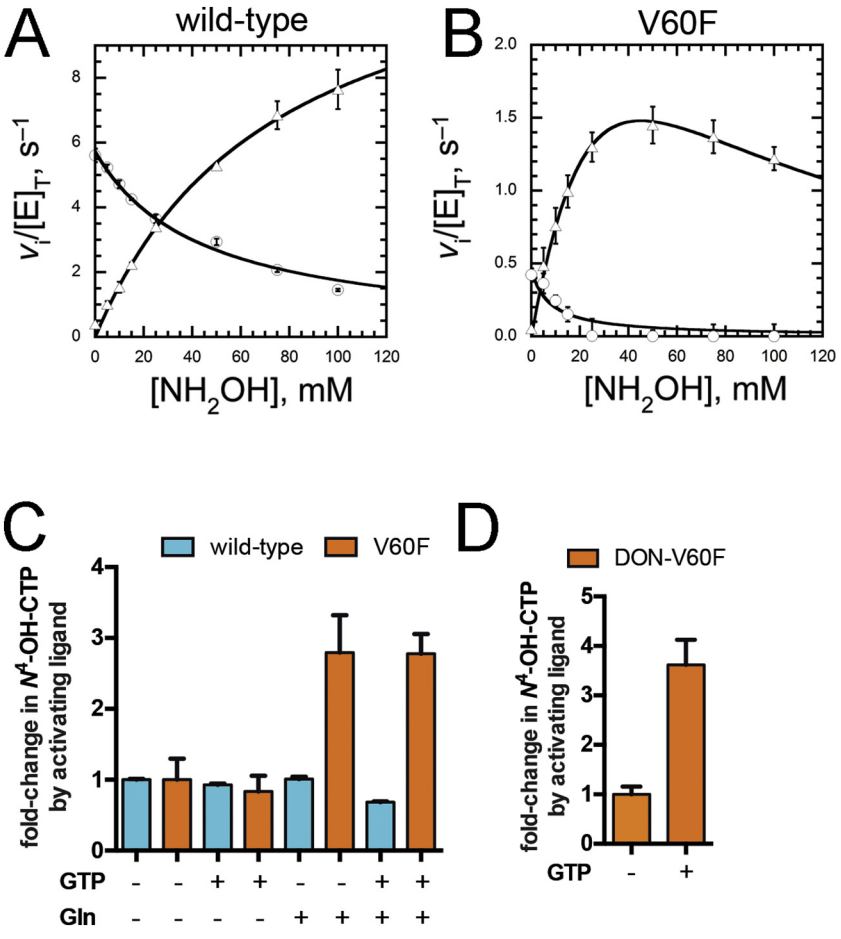

Fig. 3. Competition between nascent NH_3 and exogenous NH_2OH and the activating effects of Gln and GTP on the rates of N^4-OH-CTP formation catalyzed by wild-type, V60F, and DON-V60F *Ec*CTPSs. The rates of CTP (◯) and N^4-OH-CTP (△) formation for the wild-type (A) and V60F (B) *Ec*CTPS variants were measured in the presence of saturating concentrations of Gln (Supplementary Table S2) and varying concentrations of NH_2OH•HOAc (0–100 mM). The ionic strength was maintained at 0.10 M with NaOAc. Curves for CTP formation are fits of Eq. (7) to the initial velocity data, and curves for the formation of N^4-OH-CTP are fits of Eq. (8) (wild-type) or Eq. (9) (V60F) to the initial velocity data (see Supplementary Scheme S1). For CTP formation by wild-type *Ec*CTPS, the apparent values of ($k_{cat}^{Gln}K_S^{NH2OH}$) and K_S^{NH2OH} were 252 ± 18 mM s^{-1} and 44 ± 4 mM, respectively. For N^4-OH-CTP formation by V60F *Ec*CTPS, ($k_{cat}^{Gln}K_S^{NH2OH}$) and K_S^{NH2OH} were 4 ± 1 mM s^{-1} and 8 ± 3 mM, respectively. For N^4-OH-CTP formation by wild-type *Ec*CTPS, the apparent values of k_{cat}^{NH2OH} and K_S^{NH2OH} were 13.4 ± 0.9 s^{-1} and 74 ± 9 mM, respectively. For N^4-OH-CTP formation by V60F *Ec*CTPS the apparent values of k_{cat}^{NH2OH}, K_S^{NH2OH}, and K'_{NH2OH} were 5 ± 1 s^{-1}, 54 ± 19 mM, and 38 ± 15 mM, respectively. The activating effects of Gln and GTP on the rates of NH_2OH-dependent N^4-OH-CTP formation by wild-type (C, cyan), V60F (C, orange), or DON-V60F (D) *Ec*CTPSs were investigated by pre-incubating the enzymes with saturating concentrations of ATP and UTP (Supplementary Table S2) before initiation of the reaction with NH_2OH (100 mM for wild-type *Ec*CTPS; 25 mM for V60F and DON-V60F) and, where indicated, a saturating amount of Gln and/or GTP (Supplementary Table S2). Data are expressed as the relative change in $v_i/[E]_T$ for N^4-OH-CTP formation upon treatment with the activating ligand with respect to the control sample (i.e., Gln and GTP = 0 mM or '–').

source by V60F *Ec*CTPS, we covalently modified the active site Cys 379 of V60F with DON to mimic the structure of the glutamyl-enzyme intermediate (see Supplementary Figs. S13 and S14). Despite having an inactivated glutaminase domain, the DON-modified wild-type enzyme retains the ability to utilize exogenous NH_3 as a substrate [71, 72]. The rate constant for NH_4OAc-dependent CTP formation by DON-V60F *Ec*CTPS in the absence of GTP ($k_o = 0.25\,s^{-1}$, Table 2) was greater than the corresponding rate constant for the NH_4OAc-dependent CTP formation ($k_{cat} = 0.16\,s^{-1}$, Table 1) catalyzed by the unmodified V60F variant in the presence of GTP. This observation indicated that the basal activity was increased by the DON modification. DON-V60F *Ec*CTPS, however, was still activated by GTP and once a saturating concentration of GTP was obtained, DON-V60F *Ec*CTPS was 14-fold more active with exogenous NH_3 (derived from NH_4OAc) as a substrate ($k_{cat} = 2.2\,s^{-1}$, Table 1) than the unmodified V60F variant ($k_{cat} = 0.16\,s^{-1}$, Table 1) under identical conditions (Table 1). Indeed, NH_2OH utilization by DON-V60F *Ec*CTPS was also enhanced, but unlike the unmodified V60F variant, only in the presence of GTP (Fig. 3D), thereby suggesting that DON-V60F *Ec*CTPS was not a perfect mimic of the glutamyl-enzyme. Alkylation of V60F *Ec*CTPS by DON was also unable to completely "rescue" the ability of the variant to utilize NH_3 as a substrate since the values of k_{cat} were also 8- and 3.5-fold lower than wild-type *Ec*CTPS using either NH_4Cl or NH_4OAc as substrates, respectively. The difference in k_{cat} values with either NH_4Cl or NH_4OAc as substrates also suggests that modification by DON did not alleviate inhibition by Cl^- (Table 1).

The activation of NH_3-dependent CTP formation catalyzed by V60F and DON-V60F *Ec*CTPSs was unexpectedly dependent on GTP, which is normally an inhibitor of this activity [62]. We examined the GTP-dependent inhibition of NH_3-dependent CTP formation catalyzed by unmodified and modified (DON-*Ec*CTPS) wild-type *Ec*CTPSs as a contrast to the activating effects of GTP on the DON-V60F variant. As reported previously [53], we found that GTP inhibited DON-*Ec*CTPS ($IC_{50} = 0.08$ mM) more effectively than the unmodified enzyme ($IC_{50} \approx 3.6$ mM), but failed to ablate CTP formation entirely (Fig. 4). While DON-*Ec*CTPS had a higher apparent affinity for GTP than wild-type *Ec*CTPS based on the IC_{50} values, DON-V60F ($K_A = 0.31$ mM) had only slightly stronger affinity for GTP than unmodified V60F

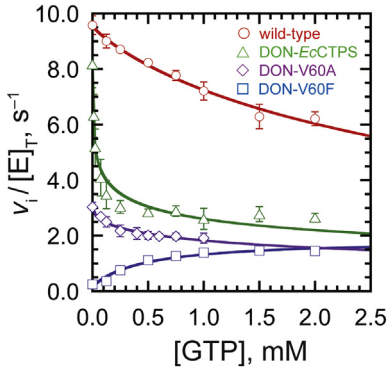

Fig. 4. Effects of GTP on NH_3-dependent CTP formation catalyzed by *Ec*CTPS variants. Unmodified wild-type (◯, red), modified wild-type (DON-*Ec*CTPS, △, green), DON-V60A (◇, violet), and DON-V60F (□, blue) *Ec*CTPSs were incubated with saturating concentrations of ATP, UTP, and NH_4OAc (Supplementary Table S2) and increasing concentrations of GTP (0–2.0 mM). The data represent the average initial velocities from three independent experiments ± SD. Curves for the wild-type, DON-*Ec*CTPS, and DON-V60A variants are fits of Eq. (4) to the initial velocity data. The IC_{50} values were 3.6 ± 0.8 mM (extrapolated) for wild-type *Ec*CTPS, 0.08 ± 0.02 mM for DON-*Ec*CTPS, and 2.2 ± 0.6 mM (extrapolated) for DON-V60A. Hill (n) values for wild-type *Ec*CTPS, DON-*Ec*CTPS, and DON-V60A variants were 0.87 ± 0.09, 0.56 ± 0.08, and 0.50 ± 0.08, respectively. In the case of DON-*Ec*CTPS, the IC_{50} was calculated using $0 \le [GTP] \le 0.25$ mM. The curve for DON-V60F is a fit of Eq. (2) and the kinetic parameters can be found in Table 2.

($K_A = 0.42$ mM) (Table 2). Together, these data indicated that the greater rate enhancement observed for DON-V60F *Ec*CTPS in the presence of GTP, relative to the unmodified V60F variant, was likely due to a conformational change arising from alkylation of the enzyme rather than an increase in affinity for GTP (although we cannot rule out the possibility that the allosteric effects of GTP may differ between the modified and unmodified V60F variants). Interestingly, the DON-*Ec*CTPS and DON-V60F variants exhibited similar activity with NH_4OAc at saturating concentrations of GTP ($v_i/[E]_T = 2.66\,s^{-1}$ and $v_i/[E]_T = 1.45\,s^{-1}$, respectively) suggesting that they both have the same levels of activity under these conditions. Assuming this was coincidence, the GTP-dependent inhibition of the DON-V60A variant was also examined in the presence of NH_4OAc. While V60A *Ec*CTPS normally has roughly 2-fold less activity than wild-type *Ec*CTPS when utilizing NH_4OAc as an NH_3 source, the DON-V60A variant still exhibited similar activity to the other modified variants at a saturating concentration of GTP (Fig. 4). These observations suggest that there is a basal rate of NH_3-dependent CTP formation by the DON-modified variants where GTP-dependent inhibition is compensated for by the GTP-dependent activation effect. That DON does not restore the affinities of V60F *Ec*CTPS for GTP, UTP, and ATP to wild-type levels, nor ameliorate the inhibition by Cl^-, suggests that the effect of DON leading to enhanced rates of NH_3-dependent CTP formation arises primarily from its effect on the NH_3 gate.

3.7. Quaternary structure of the EcCTPS variants

*Ec*CTPS is most active as a tetramer [24, 78], and changing the chemical nature of Val 60 at the dimer-dimer interface could possibly alter the ability of the V60-substituted variants to oligomerize, resulting in the diminished catalytic activity observed. For example, increasing the steric bulk (i.e., V60F or V60W) or increasing acidity (i.e., V60D) of the amino acid side chain at position 60 could have impaired assembly of the active tetramer – especially considering that some variants exhibited diminished ability to bind ATP and/or UTP that drive the oligomerization process. Moreover, the sensitivity of these variants to Cl^- was similar to that of CTPS from *L. lactis*, which has been attributed to salt-induced tetramer dissociation [68]. Hence, the apparent sensitivity of Val 60 variants to Cl^- could have caused a reduction in the pool of the active tetrameric species, and the "rescue" of V60F by Gln and DON could conceivably have arisen from an increase in the tetrameric pool of enzyme. Consequently, the oligomerization state of each *Ec*CTPS variant was analyzed by DLS using assay buffer containing saturating concentrations of UTP and ATP to induce tetramerization. For the DLS analyses, wild-type *Ec*CTPS was equilibrated without NTPs to measure the mean hydrodynamic diameter of a dimer in solution ($d_H = 8 \pm 3$ nm) as a control for non-tetramerized protein (Fig. 5). The mean hydrodynamic diameters of *Ec*CTPS tetramers were also measured in the presence of saturating concentrations of UTP and ATP with ($d_H = 15 \pm 3$ nm) or without GTP ($d_H = 15 \pm 4$ nm) to determine the hydrodynamic diameter of *Ec*CTPS tetramers under these conditions. In the presence of saturating concentrations of UTP and ATP, the V60A, V60C, V60D, and V60W variants had mean hydrodynamic diameters of 12 ± 2, 12 ± 2, 12 ± 3, and 16 ± 4 nm, respectively, indicating little or no change in oligomerization relative to wild-type *Ec*CTPS under the same conditions (Fig. 5). V60F had only a slightly lower d_H value of 13 ± 3 nm compared to wild-type *Ec*CTPS, and no increase was observed upon addition of Gln (50 mM). While GTP induced a slight increase in the d_H value to 14 ± 3 nm, the enzyme also had a d_H value of 14 ± 3 nm in the presence of both Gln and GTP suggesting that these ligands did not greatly impact oligomerization state of V60F *Ec*CTPS (Fig. 5). Furthermore, DON-V60F *Ec*CTPS, which is activated by GTP, did not exhibit any increase in mean hydrodynamic diameter following addition of GTP. Thus, the activation of the NH_3-dependent CTP formation of V60F *Ec*CTPS by Gln and GTP, and of DON-V60F *Ec*CTPS by GTP, was not due to a change in the oligomerization

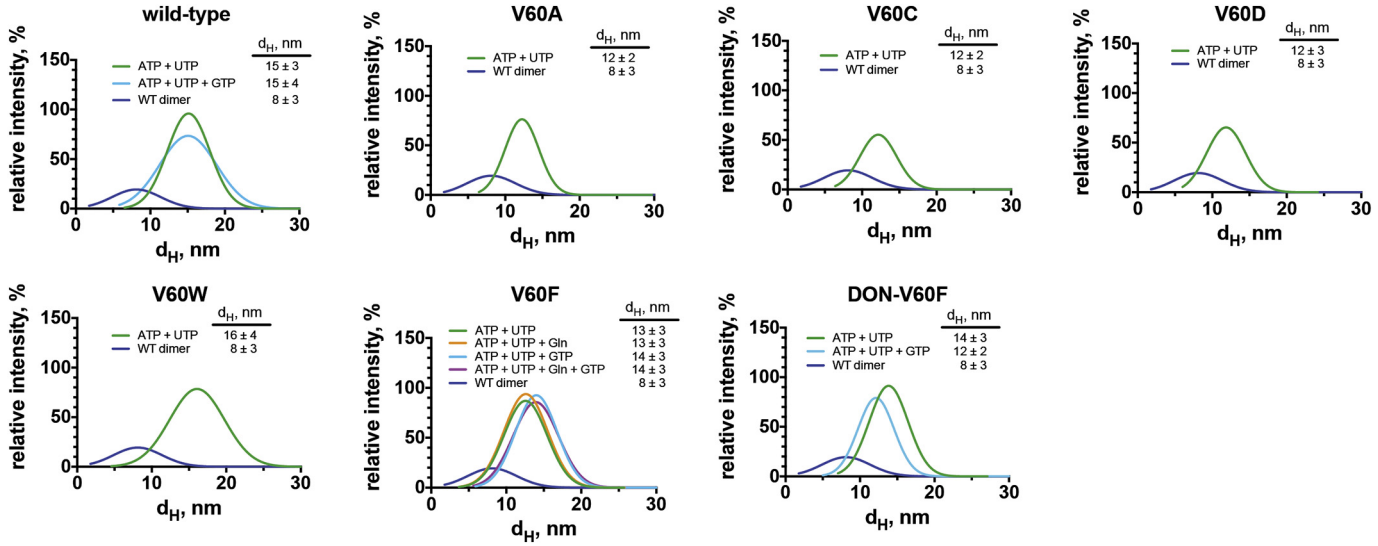

Fig. 5. DLS Analysis of the quaternary structure of wild-type and V60-substituted *Ec*CTPS variants. DLS was used to determine the mean hydrodynamic diameter (d_H) for the wild-type (WT) and V60-substituted *Ec*CTPS variants equilibrated with saturating concentrations of UTP and ATP (Supplementary Table S2) at 37 °C. Gln and/or GTP were also added, where indicated, as controls to ensure that the glutaminase-mediated activation of V60F was not caused by a shift in the oligomerization equilibrium towards the tetrameric species. Wild-type *Ec*CTPS was also equilibrated in the absence of NTPs (WT dimer) as a control for non-oligomerized (i.e., dimeric) enzyme. Data are represented as Gaussian fits to aggregate relative intensities from three experiments with the average d_H ± SD indicated for each condition. Parametric, unpaired *t*-tests conducted on the means derived from Gaussian-fits to the d_H distributions from three independent DLS experiments reveal that the d_H values for the tetramers are not statistically different; however, the d_H values for the tetramers (V60F EcCTPS (ATP + UTP) are statistically different from that of the dimer (i.e., for V60F *Ec*CTPS (ATP + UTP) vs. wild-type *Ec*CTPS, $p = 0.02$).

equilibrium to favor formation of the active tetramer. Since DLS and the kinetic assays were performed under identical conditions, this further supports the conclusion that V60F and DON-V60F *Ec*CTPSs are tetramers with localized structural perturbations consistent with constricted NH_3 tunnels.

4. Discussion

Substitutions of conserved residues often have significant detrimental consequences for catalysis by the enzyme being modified. Despite having substituted Val 60 with two naturally-occurring amino acid residues found in *Ec*CTPS homologues, no Val 60-substituted variant was completely unaffected. Even though conversion of Val 60 to the naturally-occurring Ala or Cys substitutions was relatively innocuous, the affinities of these variant enzymes for GTP were reduced (Tables 1 and 2). This effect was even more pronounced in the V60D and V60W variants, which supports previous hypotheses that the GTP-binding site is located nearby the NH_3 gate (barring any long-range effects) [26, 57, 59]. However, none of these *Ec*CTPS variants exhibited impaired NH_3 transport, and much of the reduced catalytic efficiencies resulted from a reduction in the glutaminase activity (Table 3). V60W was the most markedly affected *Ec*CTPS variant since it was unable to hydrolyze Gln, but retained the ability to utilize exogenous NH_3. Since the side chain methyl groups of Val 60 reside ~10 Å from the amide carbon of Gln in the structure if *Ec*CTPS with bound substrate (PDB ID 5TKV, [60]), it is plausible that mutation of Val 60 at the NH_3 gate may directly affect catalysis at the glutaminase site, as well as alter the conformation of the NH_3 gate to affect inter-domain NH_3 transport.

4.1. "Pinching" the NH_3 tunnel

Substitutions of Val 60 were originally prepared to investigate how NH_3 is transported between domains because the constriction shown in the crystal structures of *Ec*CTPS appears too narrow to allow the passage of NH_3 [26, 59, 60]. Assuming there is a conformational change in the tunnel that governs NH_3 transport, we attempted to perturb the function of the gate through site-directed mutagenesis to enable a kinetic interrogation of this mechanism. Remarkably, the V60F variant had limited ability to catalyze CTP formation when exogenous NH_3 was employed as the substrate, but Gln-derived NH_3 was utilized much more effectively. Furthermore, GTP was required for the utilization of exogenous NH_3 by the V60F variant despite the fact that GTP normally inhibits NH_3-dependent CTP formation [62, 79]. The requirement for GTP, and the putative proximity of its binding site to Val 60, suggested that GTP induced a conformational change in the vicinity of the gate to effect NH_3 transport. Though we were unable to obtain an X-ray structure for the V60F variant, a 100-ns molecular dynamics (MD) simulation was performed to determine how the mutation may have affected the gate. Direct comparison between the energy-minimized homology model of V60F *Ec*CTPS and the X-ray crystal structure of wild-type *Ec*CTPS [26, 59, 60] indicated that the NH_3 gate of V60F *Ec*CTPS was constricted by ~0.7 Å in radius relative to the tunnel of the wild-type enzyme (Supplementary Fig. S15). We were unable to model a tunnel within the enzyme at later times during the MD simulation due to further constriction of the gate. Additionally, the V60F *Ec*CTPS model showed that the aromatic side chain of the Phe residue interacted with the imidazole group of His 57 via an edge-on interaction for much of the simulation which may have further blocked the tunnel exit (Supplementary Fig. S16). Unfortunately, later time points also showed some localized conformational disruption (primarily domain motion about the inter-domain linker [59]) of the V60F model relative to wild-type *Ec*CTPS. However, kinetic data clearly demonstrated that nascent, but not exogenous, NH_3 could bypass this seemingly obstructed gate, suggesting that the glutaminase activity plays a role in opening the blocked gate. This mechanism of controlling the opening of the gate is reminiscent of a similar mechanism utilized by glucosamine-6-phosphate synthase (GlmS), which cannot utilize exogenous NH_3 [80]. Instead, GlmS has evolved an intrinsically blocked NH_3 tunnel that opens only during Gln hydrolysis [81]. A model summarizing the effects of the glutaminase activity, GTP binding, and modification by DON (vide infra) on the utilization of the exogenous nitrogen sources NH_3 and NH_2OH is presented in Fig. 6.

Because the efficiency (k_{cat}/K_m) of Gln-dependent CTP formation catalyzed by V60F *Ec*CTPS was reduced 176-fold, relative to wild-type

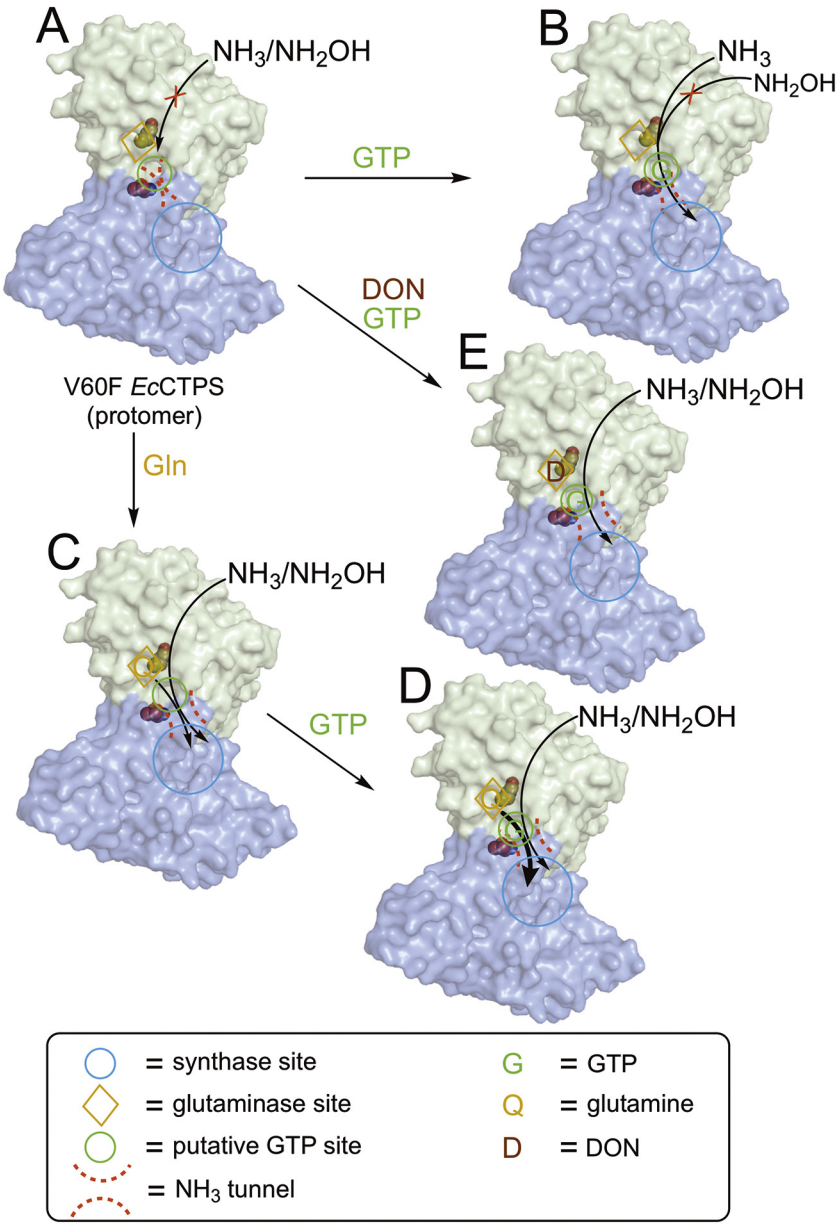

Fig. 6. Model describing the utilization of exogenous NH_3 and NH_2OH by V60F *Ec*CTPS variants. For simplicity, a single monomer is shown with the positions of the glutaminase site, GTP-binding site, NH_3 tunnel, and synthase site schematically illustrated. In the absence of GTP and Gln, the V60F variant is unable to effectively utilize exogenous NH_3 or NH_2OH as substrates (A). Upon binding of GTP, a conformational change occurs that is consistent with partial opening of the tunnel allowing for the use of exogenous NH_3, but not NH_2OH (B). Alternatively, in the presence of Gln, a conformational change occurs that permits the variant to catalyze the formation of CTP from either exogenous NH_3 or NH_2OH, or from the nascent NH_3 derived from the hydrolysis of Gln (C), the latter being promoted by the binding of GTP (thick arrow in D). Finally, mimicking the glutamyl-enzyme intermediate through modification by DON with activation by GTP (E) induces a local structural change consistent with further opening of the tunnel for more effective use of exogenous NH_3 and NH_2OH as substrates (cf. B and E). (For graphic representation, the surface representation of the monomer from wild-type *Ec*CTPS (PDB 2AD5, [26]) is shown. Cys 379 in the glutaminase active site and Val 60 (rather than Phe) are shown in sphere representation and colored yellow and red, respectively.)

*Ec*CTPS (Table 1), coupling assays were conducted with the V60F variant to determine whether the lower rates of CTP formation resulted from a leak, a bona fide blockage, or reduced rates of Gln hydrolysis. Even though there was a reduction in the intrinsic glutmainase activity of V60F *Ec*CTPS relative to wild-type *Ec*CTPS (Table 3), there existed the possibility that the tunnel was "clogged" by the rapid build-up of NH_3 at saturating concentrations of Gln such that the constricted NH_3 gate caused a "bottleneck" effect. When the concentrations of Gln were lowered to a level similar to its K_m value, or to a sub-saturating amount, the observed coupling efficiency increased such that 100% of the NH_3 produced in the glutaminase domain was utilized to generate CTP (Table 4), thereby ruling out the possibility of NH_3 leaking from the tunnel. This "bottleneck" effect was also relieved following a reduction in the concentration of GTP, even at saturating concentrations of Gln, signifying that the impaired coupling observed when both Gln and GTP are present at their saturating concentrations, is consistent with the notion that the more constricted gate of V60F *Ec*CTPS simply cannot cope with the rapid build-up of NH_3.

4.2. Opening of the V60F tunnel constriction

Evidently there was a disruption in the NH_3 tunnel of V60F *Ec*CTPS that was relieved by Gln hydrolysis (Fig. 6C) and/or GTP binding (Fig. 6B) because Gln-dependent CTP formation (i.e., transfer of nascent NH_3 through the gate) occurred much more efficiently than exogenous NH_3-dependent CTP formation. We therefore tested whether Gln and/or GTP could increase the rate of CTP formation from an exogenous nitrogen source. Since the Gln- and NH_3-derived CTP products are indistinguishable, we employed NH_2OH as an exogenous amine to mimic exogenous NH_3. We first established that both NH_2OH and nascent NH_3 compete for the same 4-phospho-UTP intermediate since *Ec*CTPS is a tetramer that exhibits half-of-the-sites reactivity with Gln [72] and subunits lacking bound Gln might still react with exogenous amines [69]. Levitski and Koshland [71] concluded that exogenous NH_3 competes with nascent NH_3 derived from Gln based on the observation that the rates of CTP formation at pH 9.25 were equal (but not additive). Willemoës [69] demonstrated directly that exogenous and nascent amines compete for the same 4-phospho-UTP in CTPS from *L. lactis*. We confirmed that nascent NH_3 and NH_2OH also compete in *Ec*CTPS by

conducting the same experiment with wild-type and V60F *Ec*CTPSs (Fig. 3A and B, respectively). The rate of N^4-OH-CTP formation was much slower with the V60F variant, possibly due to the increased bulk of NH_2OH and the presumably constricted tunnel. Consistent with the indications that the glutaminase activity was required for the passage of NH_3 in V60F *Ec*CTPS, the formation of N^4-OH-CTP was markedly enhanced in the presence of Gln (Figs. 3C and 6C). Though no GTP-dependent effect was observed, GTP may not be able to effect a great enough conformational change to enable passage of the bulkier NH_2OH through the gate as it did with exogenous NH_3 (Fig. 6B).

Gln was more effective at promoting passage of exogenous amine through the constricted tunnel of V60F *Ec*CTPS than GTP, but whether it was Gln binding or hydrolysis remained unclear. Gln is hydrolyzed in the glutaminase domain at a basal rate when GTP is absent, and this slower process may be sufficient for enhancing inter-domain NH_3 transport in V60F *Ec*CTPS. We mimicked the formation of the glutamyl-enzyme intermediate using covalent modification by DON [72] to determine whether such an acyl-enzyme intermediate mimic could induce a conformational change in the NH_3 gate to allow passage of exogenous NH_3. Indeed, it is not unreasonable to expect that the transient glutamylation of Cys 379 at the glutaminase active site could induce a conformational change (e.g., NH_3 gate opening) to facilitate the transport of each newly formed NH_3 to the synthase domain since conformational changes coordinated with ligand binding events have been demonstrated for other amidotransferases [5, 8, 12, 82, 83]. The resulting DON-V60F variant was able to catalyze CTP formation, using either NH_4Cl or NH_4OAc, at an efficiency (k_{cat}/K_m) that was ~4-fold greater than that of V60F *Ec*CTPS (Table 1), but still required GTP for activation. Unlike the unmodified V60F variant, DON-V60F *Ec*CTPS also required GTP for enhanced utilization of NH_2OH (Figs. 3D and 6D), which may be due to the static nature of the alkylated enzyme (as opposed to the hydrolyically labile acyl-enzyme intermediate) or due to an inability of GTP to facilitate opening of the NH_3 gate wide enough for the bulkier NH_2OH to pass in the absence of Gln or its mimic. The basal glutaminase activity may be sufficient for opening the tunnel of V60F *Ec*CTPS, but only when the full catalytic cycle is in progress. Nevertheless, alkylation of V60F *Ec*CTPS at Cys 379 of the glutaminase active site greatly enhanced NH_3-dependent CTP formation, supporting the notion that the glutaminase activity plays a role in opening the NH_3 gate.

That GTP activates NH_3-dependent CTP formation by V60F and DON-V60F *Ec*CTPSs at all is striking because GTP normally inhibits the utilization of exogenous NH_3 [62, 79]. Consequently, we also tested the effects of GTP on the rates of NH_3-dependent CTP formation for wild-type *Ec*CTPS, DON-*Ec*CTPS, and DON-V60A *Ec*CTPSs (Fig. 4). The DON modifications enhanced GTP binding as determined from the inhibition of wild-type *Ec*CTPS when exogenous NH_3 was employed as the nitrogen source, but never fully obviated CTP formation. The DON-*Ec*CTPS, DON-V60A, and DON-V60F variants had similar rates of CTP formation at saturating concentrations of GTP indicating that modification of V60F *Ec*CTPS by DON, by and large, "rescued" the enzyme by restoring near-wild-type levels of activity under these conditions (Fig. 4). The slightly lower rates of CTP formation catalyzed by the DON-V60A and DON-V60F variants with respect to DON-*Ec*CTPS are likely due to the slight inhibitory effects of acetate. Although it seems counter-intuitive, it may be that DON-V60F *Ec*CTPS (and V60F *Ec*CTPS) is inhibited by GTP, i.e., GTP may have dual, separable effects on DON-V60F *Ec*CTPS compared to DON-*Ec*CTPS, with both enzymes inhibited similarly but with a V60F-specific effect that relieves the constriction in the NH_3 tunnel.

4.3. Concluding remarks

Several studies have been conducted to understand how amidotransferases coordinate NH_3 transport with "downstream" amidoligation reactions in a synthase domain, generally through site-directed mutagenesis and subsequent kinetic analyses. Carbamoyl phosphate synthase (CPS) [84–86], glutamine-dependent NAD^+ synthetase (NadE) [14], GlmS [80, 81], phosphoribosylformylglycinamidine synthase [15], Gln phosphoribosylpyrophsphate amidotransferase [87], and imidazole glycerol phosphate synthase [88, 89] are just a few examples of amidotransferases that have been extensively studied and structurally characterized with respect to their ability to synchronize multiple reactions. The tunnel of NadE contains several aperture-like constrictions that open/close depending on what combination of ligands are bound, and substitution of the conserved Leu 489 by Phe reduced inter-domain coupling efficiency [14]. Mutation ($_{\alpha}$P360A/$_{\alpha}$H361A/$_{\beta}$R265A) of CPS resulted in a perforation of its NH_3 tunnel leading to nascent NH_3 leaking from the tunnel; however, full catalytic activity with exogenous NH_3 was retained [85]. In the present study, we obtained an unusual result in that a single-amino acid substitution blocked the use of exogenous NH_3, but retained Gln-dependent activity, suggesting that opening of the NH_3 gate is effected, in part, by the "upstream" glutaminase activity.

X-Ray crystal structures of *Ec*CTPS are challenging to obtain as evidenced by the dearth of reported structures [26, 59, 60]; and no high-resolution structures of *Ec*CTPS have yet been solved with GTP bound. Although this leaves us without direct observation of how the Val 60 side chain substitutions affect the overall structure and/or conformation of *Ec*CTPS, our extensive mutational and kinetic analyses indicate that Val 60 plays a central role that impacts glutaminase activity, NTP binding, inhibition by Cl^-, and coupling of reactions between domains. Clearly, substitutions at position 60 produce a local disruption of structure that affects a variety of functions. Most significantly, however, the local disruption of structure resulting from the slight increase in steric bulk due to the substitution of Val 60 with Phe was sufficient to induce an effect that was consistent with "pinching" of the NH_3 tunnel, permitting us to uncover the relationship between processes that synchronize the transfer of NH_3 from the glutaminase domain to the synthase domain. Though wild-type *Ec*CTPS does not require Gln hydrolysis to efficiently utilize exogenous NH_3, presumably because its NH_3 gate is more open, the V60F variant has just enough of a constriction in the NH_3 gate to furnish us with an enzyme that reveals how the glutaminase activity and GTP-dependent activation can act in concert to mediate inter-domain NH_3 transport.

Acknowledgements

We thank Dr. Alejandro Cohen of the Dalhousie Faculty of Medicine Proteomics Facility for his assistance with mass spectrometry experiments.

Funding

This work was supported by an operating grant from the Canadian Institutes of Health Research (no. 114895, S.L.B.) and a Scotia Support Grant from the Nova Scotia Heath Research Foundation (no. 140; S.L.B.). G.D.M. is a trainee in the Cancer Research Training Program of the Beatrice Hunter Cancer Research Institute, with funds provided by Craig's Cause Pancreatic Cancer Society, a CIBC Graduate Scholarship in Medical Research, and The Terry Fox Research Institute.

Notes

The authors declare no competing financial interest.

Appendix A. Supplementary data

Supplementary data to this article can be found online at https://doi.org/10.1016/j.bbagen.2018.08.008.

References

[1] A. Gora, J. Brezovsky, J. Damborsky, Gates of enzymes, Chem. Rev. 113 (2013) 5871–5923.
[2] L.J. Kingsley, M.A. Lill, Substrate tunnels in enzymes: structure-function relationships and computational methodology, Proteins 83 (2015) 599–611.
[3] F. Massiere, M.A. Badet-Denisot, The mechanism of glutamine-dependent amidotransferases, Cell. Mol. Life Sci. 54 (1998) 205–222.
[4] F.M. Raushel, J.B. Thoden, H.M. Holden, The amidotransferase family of enzymes: molecular machines for the production and delivery of ammonia, Biochemistry 38 (1999) 7891–7899.
[5] X. Huang, H.M. Holden, F.M. Raushel, Channeling of substrates and intermediates in enzyme-catalyzed reactions, Annu. Rev. Biochem. 70 (2001) 149–180.
[6] F.M. Raushel, J.B. Thoden, H.M. Holden, Enzymes with molecular tunnels, Acc. Chem. Res. 36 (2003) 539–548.
[7] A. Weeks, L. Lund, F.M. Raushel, Tunneling of intermediates in enzyme-catalyzed reactions, Curr. Opin. Chem. Biol. 10 (2006) 465–472.
[8] S. Mouilleron, B. Golinelli-Pimpaneau, Conformational changes in ammonia-channeling glutamine amidotransferases, Curr. Opin. Struct. Biol. 17 (2007) 653–664.
[9] M.G. Plach, F. Semmelmann, F. Busch, M. Busch, L. Heizinger, V.H. Wysocki, R. Merkl, R. Sterner, Evolutionary diversification of protein-protein interactions by interface add-ons, Proc. Natl. Acad. Sci. U. S. A. 114 (2017) E8333–E8342.
[10] H. Zalkin, The amidotransferases, Adv. Enzymol. Relat. Areas Mol. Biol. 66 (1993) 203–309.
[11] F. Busch, C. Rajendran, K. Heyn, S. Schlee, R. Merkl, R. Sterner, Ancestral tryptophan synthase reveals functional sophistication of primordial enzyme complexes, Cell Chem. Biol. 23 (2016) 709–715.
[12] J.L. Johnson, J.K. West, A.D. Nelson, G.D. Reinhart, Resolving the fluorescence response of *Escherichia coli* carbamoyl phosphate synthetase: mapping intra- and intersubunit conformational changes, Biochemistry 46 (2007) 387–397.
[13] R.H. van den Heuvel, D. Ferrari, R.T. Bossi, S. Ravasio, B. Curti, M.A. Vanoni, F.J. Florencio, A. Mattevi, Structural studies on the synchronization of catalytic centers in glutamate synthase, J. Biol. Chem. 277 (2002) 24579–24583.
[14] W. Chuenchor, T.I. Doukov, M. Resto, A. Chang, B. Gerratana, Regulation of the intersubunit ammonia tunnel in *Mycobacterium tuberculosis* glutamine-dependent NAD^+ synthetase, Biochem. J. 443 (2012) 417–426.
[15] A.S. Tanwar, D.J. Sindhikara, F. Hirata, R. Anand, Determination of the formylglycinamide ribonucleotide amidotransferase ammonia pathway by combining 3D-RISM theory with experiment, ACS Chem. Biol. 10 (2015) 698–704.
[16] B. Ghosh, V.D. Goyal, Gating role of His 72 in TmPurL enzyme uncovered by structural analyses and molecular dynamics simulations, Bioorg. Med. Chem. Lett. 26 (2016) 5644–5649.
[17] L. Zhao, U.M. Rathnayake, S.W. Dewage, W.N. Wood, A.J. Veltri, G.A. Cisneros, T.L. Hendrickson, Characterization of tunnel mutants reveals a catalytic step in ammonia delivery by an aminoacyl-tRNA amidotransferase, FEBS Lett. 590 (2016) 3122–3132.
[18] M.L. Weng, H. Zalkin, Structural role for a conserved region in the CTP synthetase glutamine amide transfer domain, J. Bacteriol. 169 (1987) 3023–3028.
[19] W. von der Saal, P.M. Anderson, J.J. Villafranca, Mechanistic investigations of *Escherichia coli* cytidine-5′-triphosphate synthetase. Detection of an intermediate by positional isotope exchange experiments, J. Biol. Chem. 260 (1985) 14993–14997.
[20] D.A. Lewis, J.J. Villafranca, Investigation of the mechanism of CTP synthetase using rapid quench and isotope partitioning methods, Biochemistry 28 (1989) 8454–8459.
[21] M. Willemoës, B.W. Sigurskjold, Steady-state kinetics of the glutaminase reaction of CTP synthase from *Lactococcus lactis*, Eur. J. Biochem. 269 (2002) 4772–4779.
[22] C.W. Long, A.B. Pardee, Cytidine triphosphate synthetase of *Escherichia coli* B. I. Purification and kinetics, J. Biol. Chem. 242 (1967) 4715–4721.
[23] A. Levitzki, D.E. Koshland Jr., Negative cooperativity in regulatory enzymes, Proc. Natl. Acad. Sci. U. S. A. 62 (1969) 1121–1128.
[24] A. Levitzki, D.E. Koshland Jr., Ligand-induced dimer-to-tetramer transformation in cytosine triphosphate synthetase, Biochemistry 11 (1972) 247–253.
[25] A. Pappas, W.L. Yang, T.S. Park, G.M. Carman, Nucleotide-dependent tetramerization of CTP synthetase from *Saccharomyces cerevisiae*, J. Biol. Chem. 273 (1998) 15954–15960.
[26] J.A. Endrizzi, H. Kim, P.M. Anderson, E.P. Baldwin, Mechanisms of product feedback regulation and drug resistance in cytidine triphosphate synthetases from the structure of a CTP-inhibited complex, Biochemistry 44 (2005) 13491–13499.
[27] M. Bakovic, M.D. Fullerton, V. Michel, Metabolic and molecular aspects of ethanolamine phospholipid biosynthesis: the role of CTP:phosphoethanolamine cytidylyltransferase (Pcyt2), Biochem. Cell Biol. 85 (2007) 283–300.
[28] Y.F. Chang, G.M. Carman, CTP synthetase and its role in phospholipid synthesis in the yeast *Saccharomyces cerevisiae*, Prog. Lipid Res. 47 (2008) 333–339.
[29] D.B. Ostrander, D.J. O'Brien, J.A. Gorman, G.M. Carman, Effect of CTP synthetase regulation by CTP on phospholipid synthesis in *Saccharomyces cerevisiae*, J. Biol. Chem. 273 (1998) 18992–19001.
[30] S. Hatse, E. De Clercq, J. Balzarini, Role of antimetabolites of purine and pyrimidine nucleotide metabolism in tumor cell differentiation, Biochem. Pharmacol. 58 (1999) 539–555.
[31] E. De Clercq, Antiviral agents: characteristic activity spectrum depending on the molecular target with which they interact, Adv. Virus Res. 42 (1993) 1–55.
[32] A. Fijolek, A. Hofer, L. Thelander, Expression, purification, characterization, and *in vivo* targeting of trypanosome CTP synthetase for treatment of African sleeping sickness, J. Biol. Chem. 282 (2007) 11858–11865.
[33] E.F. Hendriks, W.J. O'Sullivan, T.S. Stewart, Molecular cloning and characterization of the *Plasmodium falciparum* cytidine triphosphate synthetase gene, Biochim. Biophys. Acta 1399 (1998) 213–218.
[34] R.L. Lim, W.J. O'Sullivan, T.S. Stewart, Isolation, characterization and expression of the gene encoding cytidine triphosphate synthetase from *Giardia intestinalis*, Mol. Biochem. Parasitol. 78 (1996) 249–257.
[35] A. Hofer, D. Steverding, A. Chabes, R. Brun, L. Thelander, *Trypanosoma brucei* CTP synthetase: a target for the treatment of African sleeping sickness, Proc. Natl. Acad. Sci. U. S. A. 98 (2001) 6412–6416.
[36] C.H. Steeves, S.L. Bearne, Activation and inhibition of CTP synthase from *Trypanosoma brucei*, the causative agent of African sleeping sickness, Bioorg. Med. Chem. Lett. 21 (2011) 5188–5190.
[37] J.O. de Souza, A. Dawson, W.N. Hunter, An improved model of the *Trypanosoma brucei* CTP synthetase glutaminase domain: acivicin complex, ChemMedChem 12 (2017) 577–579.
[38] H.Y. Narvaez-Ortiz, A.J. Lopez, N. Gupta, B.H. Zimmermann, A CTP synthase undergoing stage-specific spatial expression is essential for the survival of the intracellular parasite *Toxoplasma gondii*, Front. Cell. Infect. Microbiol. 8 (2018) 83.
[39] A.C. Verschuur, A.H. Van Gennip, R. Leen, P.A. Voute, J. Brinkman, A.B. Van Kuilenburg, Cyclopentenyl cytosine increases the phosphorylation and incorporation into DNA of 1-β-D-arabinofuranosyl cytosine in a human T-lymphoblastic cell line, Int. J. Cancer 98 (2002) 616–623.
[40] E. Martin, N. Palmic, S. Sanquer, C. Lenoir, F. Hauck, C. Mongellaz, S. Fabrega, P. Nitschké, M.D. Esposti, J. Schwartzentruber, N. Taylor, J. Majewski, N. Jabado, R.F. Wynn, C. Picard, A. Fischer, P.D. Arkwright, S. Latour, CTP synthase 1 deficiency in humans reveals its central role in lymphocyte proliferation, Nature 510 (2014) 288–292.
[41] M.G. Choi, T.S. Park, G.M. Carman, Phosphorylation of *Saccharomyces cerevisiae* CTP synthetase at Ser424 by protein kinases a and C regulates phosphatidylcholine synthesis by the CDP-choline pathway, J. Biol. Chem. 278 (2003) 23610–23616.
[42] T.S. Park, D.J. O'Brien, G.M. Carman, Phosphorylation of CTP Synthetase on Ser36, Ser330, Ser354, and Ser454 regulates the levels of CTP and phosphatidylcholine synthesis in *Saccharomyces cerevisiae*, J. Biol. Chem. 278 (2003) 20785–20794.
[43] Y.F. Chang, S.S. Martin, E.P. Baldwin, G.M. Carman, Phosphorylation of human CTP synthetase 1 by protein kinase C: identification of Ser(462) and Thr(455) as major sites of phosphorylation, J. Biol. Chem. 282 (2007) 17613–17622.
[44] M.J. Higgins, P.R. Graves, L.M. Graves, Regulation of human cytidine triphosphate synthetase 1 by glycogen synthase kinase 3, J. Biol. Chem. 282 (2007) 29493–29503.
[45] R.M. Barry, A.F. Bitbol, A. Lorestani, E.J. Charles, C.H. Habrian, J.M. Hansen, H.J. Li, E.P. Baldwin, N.S. Wingreen, J.M. Kollman, Z. Gitai, Large-scale filament formation inhibits the activity of CTP synthetase, elife 3 (2014) e03638.
[46] M. Ingerson-Mahar, A. Briegel, J.N. Werner, G.J. Jensen, Z. Gitai, The metabolic enzyme CTP synthase forms cytoskeletal filaments, Nat. Cell Biol. 12 (2010) 739–746.
[47] K.M. Gou, C.C. Chang, Q.J. Shen, L.Y. Sung, J.L. Liu, CTP synthase forms cytoophidia in the cytoplasm and nucleus, Exp. Cell Res. 323 (2014) 242–253.
[48] T.I. Strochlic, K.P. Stavrides, S.V. Thomas, E. Nicolas, A.M. O'Reilly, J.R. Peterson, Ack kinase regulates CTP synthase filaments during *Drosophila* oogenesis, EMBO Rep. 15 (2014) 1184–1191.
[49] C. Noree, E. Monfort, A.K. Shiau, J.E. Wilhelm, Common regulatory control of CTP synthase enzyme activity and filament formation, Mol. Biol. Cell 25 (2014) 2282–2290.
[50] P.Y. Wang, W.C. Lin, Y.C. Tsai, M.L. Cheng, Y.H. Lin, S.H. Tseng, A. Chakraborty, L.M. Pai, Regulation of CTP synthase filament formation during DNA endoreplication in *Drosophila*, Genetics 201 (2015) 1511–1523.
[51] G.N. Aughey, S.J. Grice, J.L. Liu, The interplay between Myc and CTP synthase in Drosophila, PLoS Genet. 12 (2016) e1005867.
[52] G.D. McCluskey, S.L. Bearne, Analysis of bacterial CTP synthase filaments formed in the presence of the chemotherapeutic metabolite gemcitabine-5′-triphosphate, J. Mol. Biol. 430 (2018) 1201–1217.
[53] A. Levitzki, D.E. Koshland Jr., Role of an allosteric effector. Guanosine triphosphate activation in cytosine triphosphate synthetase, Biochemistry 11 (1972) 241–246.
[54] A. Iyengar, S.L. Bearne, Aspartate 107 and leucine 109 facilitate efficient coupling of glutamine hydrolysis to CTP synthesis by *E. coli* CTP synthase, Biochem. J. 369 (2003) 497–507.
[55] M. Willemoës, Thr-431 and Arg-433 are part of a conserved sequence motif of the glutamine amidotransferase domain of CTP synthases and are involved in GTP activation of the *Lactococcus lactis* enzyme, J. Biol. Chem. 278 (2003) 9407–9411.
[56] D. Simard, K.A. Hewitt, F. Lunn, A. Iyengar, S.L. Bearne, Limited proteolysis of *Escherichia coli* cytidine-5′-triphosphate synthase. Identification of residues required for CTP formation and GTP-dependent activation of glutamine hydrolysis, Eur. J. Biochem. 270 (2003) 2195–2206.
[57] F.A. Lunn, S.L. Bearne, Alternative substrates for wild-type and L109A *E. coli* CTP synthases. Kinetic evidence for a constricted ammonia tunnel, Eur. J. Biochem. 271 (2004) 4204–4212.
[58] S.L. Bearne, O. Hekmat, J.E. MacDonnell, Inhibition of *Escherichia coli* CTP synthase by glutamate γ-semialdehyde and the role of the allosteric effector GTP in glutamine hydrolysis, Biochem. J. 356 (2001) 223–232.
[59] J.A. Endrizzi, H. Kim, P.M. Anderson, E.P. Baldwin, Crystal structure of *Escherichia coli* cytidine triphosphate synthetase, a nucleotide-regulated glutamine amidotransferase/ATP-dependent amidoligase fusion protein and homologue of anticancer and antiparasitic drug targets, Biochemistry 43 (2004) 6447–6463.
[60] E.M. Lynch, D.R. Hicks, M. Shepherd, J.A. Endrizzi, A. Maker, J.M. Hansen, R.M. Barry, Z. Gitai, E.P. Baldwin, J.M. Kollman, Human CTP synthase filament structure reveals the active enzyme conformation, Nat. Struct. Biol. 24 (2017) 507–514.

[61] G. Mori, L.R. Chiarelli, M. Esposito, V. Makarov, M. Bellinzoni, R.C. Hartkoorn, G. Degiacomi, F. Boldrin, S. Ekins, A.L. de Jesus Lopes Ribeiro, L.B. Marino, I. Centárová, Z. Svetlíková, J. Blaško, E. Kazakova, A. Lepioshkin, N. Barilone, G. Zanoni, A. Porta, M. Fondi, R. Fani, A.R. Baulard, K. Mikušová, P.M. Alzari, R. Manganelli, L.P. de Carvalho, G. Riccardi, S.T. Cole, M.R. Pasca, Thiophenecarboxamide derivatives activated by EthA kill *Mycobacterium tuberculosis* by inhibiting the CTP synthetase PyrG, Chem. Biol. 22 (2015) 917–927.
[62] J.E. MacDonnell, F.A. Lunn, S.L. Bearne, Inhibition of *E. coli* CTP synthase by the "positive" allosteric effector GTP, Biochim. Biophys. Acta 2004 (1699) 213–220.
[63] H. Zalkin, CTP synthetase, Methods Enzymol. 113 (1985) 282–287.
[64] C.W. Kammeyer, D.R. Whitman, Quantum mechanical calculation of molecular radii. I. Hydrides of elements of periodic groups IV through VII, J. Chem. Phys. 56 (1972) 4419–4421.
[65] E. Gasteiger, A. Gattiker, C. Hoogland, I. Ivanyi, R.D. Appel, A. Bairoch, ExPASy: the proteomics server for in-depth protein knowledge and analysis, Nucleic Acids Res. 31 (2003) 3784–3788.
[66] A. Iyengar, S.L. Bearne, An assay for CTP synthetase glutaminase activity using high performance liquid chromatography, Anal. Biochem. 308 (2002) 396–400.
[67] T. Higuchi, C.H. Barnstein, Hydroxylammonium acetate as carbonyl reagent, Anal. Chem. 28 (1956) 1022–1025.
[68] M. Willemoës, S. Larsen, Substrate inhibition of *Lactococcus lactis* cytidine-5′-triphosphate synthase by ammonium chloride is enhanced by salt-dependent tetramer association, Arch. Biochem. Biophys. 413 (2003) 17–22.
[69] M. Willemoës, Competition between ammonia derived from internal glutamine hydrolysis and hydroxylamine present in the solution for incorporation into UTP as catalysed by *Lactococcus lactis* CTP synthase, Arch. Biochem. Biophys. 424 (2004) 105–111.
[70] N.E. Good, Activation of the Hill reaction by amines, Biochim. Biophys. Acta 40 (1960) 502–517.
[71] A. Levitzki, D.E. Koshland Jr., Cytidine triphosphate synthetase. Covalent intermediates and mechanisms of action, Biochemistry 10 (1971) 3365–3371.
[72] A. Levitzki, W.B. Stallcup, D.E. Koshland Jr., Half-of-the-sites reactivity and the conformational states of cytidine triphosphate synthetase, Biochemistry 10 (1971) 3371–3378.
[73] N. Guex, M.C. Peitsch, SWISS-MODEL and the Swiss-PdbViewer: an environment for comparative protein modeling, Electrophoresis 18 (1997) 2714–2723.
[74] H.J.C. Berendsen, D. van der Spoel, R. van Drunen, GROMACS: a message-passing parallel molecular dynamics implementation, Comput. Phys. Commun. 91 (1995) 43–56.
[75] B. Kozlíková, E. Šebestová, V. Šustr, J. Brezovský, O. Strnad, L. Daniel, D. Bednář, A. Pavelka, M. Maňák, M. Bezděka, P. Beneš, M. Kotry, A.W. Gora, J. Damborský, J. Sochor, CAVER analyst 1.0: graphic tool for interactive visualization and analysis of tunnels and channels in protein structures, Bioinformatics 30 (2014) 2684–2685.
[76] M. Nagar, B.N. Wyatt, M.St. Maurice, S.L. Bearne, Inactivation of mandelate racemase by 3-hydroxypyruvate reveals a potential mechanistic link between enzyme superfamilies, Biochemistry 54 (2015) 2747–2757.
[77] M. Willemoës, A. Mølgaard, E. Johansson, J. Martinussen, Lid L11 of the glutamine amidotransferase domain of CTP synthase mediates allosteric GTP activation of glutaminase activity, FEBS J. 272 (2005) 856–864.
[78] J.G. Robertson, Determination of subunit dissociation constants in native and inactivated CTP synthetase by sedimentation equilibrium, Biochemistry 34 (1995) 7533–7541.
[79] C. Habrian, A. Chandrasekhara, B. Shahrvini, B. Hua, J. Lee, R. Jesinghaus, R. Barry, Z. Gitai, J. Kollman, E.P. Baldwin, Inhibition of *Escherichia coli* CTP synthetase by NADH and other nicotinamides and their mutual interactions with CTP and GTP, Biochemistry 55 (2016) 5554–5565.
[80] A. Teplyakov, G. Obmolova, B. Badet, M.A. Badet-Denisot, Channeling of ammonia in glucosamine-6-phosphate synthase, J. Mol. Biol. 313 (2001) 1093–1102.
[81] S. Mouilleron, M.A. Badet-Denisot, Glutamine binding opens the ammonia channel and activates glucosamine-6P synthase, J. Biol. Chem. 281 (2006) 4404–4412.
[82] S. Chen, J.W. Burgner, J.M. Krahn, J.L. Smith, H. Zalkin, Tryptophan fluorescence monitors multiple conformational changes required for glutamine phosphoribosylpyrophosphate amidotransferase interdomain signaling and catalysis, Biochemistry 38 (1999) 11659–11669.
[83] J.Y. Bhat, R. Venkatachala, H. Balaram, Substrate-induced conformational changes in *Plasmodium falciparum* guanosine monophosphate synthetase, FEBS J. 278 (2011) 3756–3768.
[84] J. Kim, F.M. Raushel, Allosteric control of the oligomerization of carbamoyl phosphate synthetase from *Escherichia coli*, Biochemistry 40 (2001) 11030–11036.
[85] J. Kim, F.M. Raushel, Perforation of the tunnel wall in carbamoyl phosphate synthetase derails the passage of ammonia between sequential active sites, Biochemistry 43 (2004) 5334–5340.
[86] L.S. Mullins, F.M. Raushel, Channeling of ammonia through the intermolecular tunnel contained within carbamoyl phosphate synthetase, J. Am. Chem. Soc. 121 (1999) 3803–3804.
[87] J.M. Krahn, J.H. Kim, M.R. Burns, R.J. Parry, H. Zalkin, J.L. Smith, Coupled formation of an amidotransferase interdomain ammonia channel and a phosphoribosyltransferase active site, Biochemistry 36 (1997) 11061–11068.
[88] R.E. Amaro, R.S. Myers, V.J. Davisson, Z.A. Luthey-Schulten, Structural elements in IGP synthase exclude water to optimize ammonia transfer, Biophys. J. 89 (2005) 475–487.
[89] R.S. Myers, R.E. Amaro, Z.A. Luthey-Schulten, V.J. Davisson, Reaction coupling through interdomain contacts in imidazole glycerol phosphate synthase, Biochemistry 44 (2005) 11974–11985.
[90] G.D. McCluskey, S. Mohamady, S.D. Taylor, S.L. Bearne, Exploring the potent inhibition of CTP synthase by gemcitabine-5′-triphosphate, ChemBioChem 17 (2016) 2240–2249.
[91] T.J. Wheeler, J. Clements, R.D. Finn, Skylign: a tool for creating informative, interactive logos representing sequence alignments and profile hidden Markov models, BMC Bioinforma. 15 (2014), https://doi.org/10.1186/1471-2105-1115-1187.
[92] R.D. Finn, P. Coggill, R.Y. Eberhardt, S.R. Eddy, J. Mistry, A.L. Mitchell, S.C. Potter, M. Punta, M. Qureshi, A. Sangrador-Vegas, G.A. Salazar, J. Tate, A. Bateman, The Pfam protein families database: towards a more sustainable future, Nucleic Acids Res. 44 (D1) (2016) D279–D285.
[93] F. Sievers, D.G. Higgins, Clustal omega, accurate alignment of very large numbers of sequences, Methods Mol. Biol. 1079 (2014) 105–116.